Phosphoprotein Phosphatase Activity Positively Regulates Oligomeric Pyrin to Trigger Inflammasome Assembly in Phagocytes

Haleema S. Malik[1], Flora Magnotti[3], Nicole A. Loeven[1], Jose M. Delgado[2], Arminja N. Kettenbach[1,2], Thomas Henry[3] and James B. Bliska[1]

[1]Department of Microbiology and Immunology, and [2]Department of Biochemistry and Cell Biology, Geisel School of Medicine at Dartmouth, Hanover NH, USA

[2]Norris Cotton Cancer Center, Lebanon, NH, USA.

[3]CIRI, Centre International de Recherche en Infectiologie, Inserm U1111, Université Claude Bernard Lyon 1, CNRS, UMR5308, ENS de Lyon, Univ Lyon, Lyon, France

Correspondence:
James B. Bliska
Department of Microbiology and Immunology, Geisel School of Medicine at Dartmouth, 66 College Street, Hanover NH, 03755 USA
Email: james.bliska@dartmouth.edu

Classification: Biological Sciences, Immunology and Inflammation

Key words: Phosphoprotein phosphatase, Pyrin, Inflammasome, Phagocyte

ABSTRACT:

Pyrin is a pattern-recognition receptor in phagocytes that triggers capase-1 inflammasome assembly in response to bacterial toxins and effectors that inactivate RhoA. Pyrin contains oligomerization domains and is negatively regulated by phosphorylation of two residues, S205 and S241 (murine) or S208 and S242 (human), via the kinases PKN1/2, which are activated by RhoA. Familial Mediterranean Fever (FMF) is caused by phagocyte production of pyrin gain of function variants, which have a lower threshold for inflammasome assembly upon RhoA-PKN axis inhibition. Inactivation of the RhoA-PKN axis removes negative regulation but a phosphoprotein phosphatase (PPP) is needed to positively regulate pyrin. No PPP that dephosphorylates pyrin has been identified, oligomerization of murine pyrin has not been studied, and the phosphorylation status of oligomeric pyrin is unknown. We used murine macrophages and FMF patient's monocytes combined with the use of bacterial and chemical inhibitors, native PAGE, phospho-specific antibodies and siRNA knockdowns to determine if a PPP positively regulates oligomeric pyrin. Results with inhibitors indicate that PPP activity is required to dephosphorylate murine and human pyrin in wild type or FMF patient's phagocytes. Findings from native PAGE show that murine pyrin forms oligomers that are phosphorylated on S205 prior to RhoA inactivation. Inhibitor treatment causes reduced mobility of murine pyrin on native PAGE and hyperphosphorylation of S242 in human pyrin, suggesting a PPP constitutively counterbalances PKN to keep the second site hypophosphorylated. Data from siRNA knockdown experiments implicate PP2A in dephosphorylation of S205 and positive regulation of pyrin in response to RhoA inactivation.

SIGNIFICANCE:

It is important to understand how pyrin promotes immune responses against pathogens and autoinflammation in FMF and a deeper understanding of inflammasome regulation will aid in this goal. The negative regulation mechanism by the RhoA-PKN axis is established but how inflammasome assembly is controlled by pyrin oligomerization and positively regulated by PPP activity is poorly understood. Results of this study shed new light on pyrin oligomerization and demonstrate that PPP activity is required to dephosphorylate pyrin and trigger inflammasome assembly in murine and human phagocytes in response to RhoA-inactivating bacterial toxins and effectors or a PKN inhibitor in the context of FMF. The identification of a specific role for PP2A may inform the development of new therapeutics for FMF.

61 INTRODUCTION

62 Numerous Gram-negative bacterial pathogens encode type III secretion systems (T3SSs) that
63 are essential for virulence (1). T3SSs translocate effectors into or across the plasma membrane
64 and into the eukaryotic cytosol during bacterial-host cell contact. Translocated effectors can inhibit
65 innate immune responses to promote pathogenesis (1, 2). Host cells can sense perturbations
66 caused by T3SSs and/or effectors and produce compensatory innate immune responses to
67 counteract infection by pathogens (3, 4). Perturbations induced by T3SSs and/or effectors in
68 macrophages infected with bacterial pathogens can result in the assembly of caspase-1
69 inflammasomes (5, 6). Inflammasomes are multimeric complexes that are assembled in response
70 to various danger signals in the cell cytosol and serve as a molecular platform for the recruitment
71 and maturation of caspase-1 into its active form (5, 6). Active caspase-1 cleaves gasdermin-D
72 (GSDMD), pro-IL-1β and pro-IL-18 (7-9). The N-terminal domain of GSDMD forms pores in the
73 plasma membrane which allow for release of mature IL-1β and IL-18 (7-9). GSDMD pores can
74 also promote cell death, termed pyroptosis, resulting in the release of additional pro-inflammatory
75 molecules (10). Pyroptosis amplifies the immune response by restricting growth of bacteria and
76 facilitating bacterial clearance by neutrophils (7). Virulent bacterial pathogens can inhibit caspase-
77 1 inflammasomes in host cells to counteract protective immune responses mediated by IL-1β, IL-
78 18 and pyroptosis (11).

79 *Yersinia* species are Gram-negative bacterial pathogens that cause invasive human infections
80 ranging in severity from plague (*Y. pestis*) to mesenteric lymphadenitis (*Y. pseudotuberculosis,*
81 *Yptb*). These bacteria replicate in lymphoid tissues as extracellular microcolonies and require a
82 plasmid-encoded T3SS for virulence (12). The T3SS delivers seven effectors called *Yersinia* outer
83 proteins (Yops) into the cytosol of phagocytes that are in contact with *Yersinia* (12). The effectors
84 inhibit key host cell processes, including phagocytosis and proinflammatory cytokine production
85 (13). For example, YopE and YopT inhibit phagocytosis by inactivating Rho GTPases, including
86 RhoA (13). YopE mimics a Rho GTPase activating protein (GAP) to accelerate GTP hydrolysis to
87 GDP in RhoA (14), while YopT is a cysteine protease which cleaves RhoA at its C-terminus so
88 that it is released from the membrane (15). Two effectors that are essential virulence factors inhibit
89 inflammasome activation: YopM, a leucine-rich repeat (LRR)-containing protein (16-18) and YopK
90 (19, 20). YopM inhibits the pyrin inflammasome (17, 18). YopK interacts with *Yersinia* translocon
91 components to limit activation of NLRP3 and NLRC4 inflammasomes (19).

92 Inactivation of RhoA by YopE or YopT in macrophages triggers assembly of the pyrin
93 inflammasome as a compensatory protective innate immune response (17, 18, 21, 22). Pyrin is a
94 cytosolic pattern recognition receptor (PRR) which specifically senses pathogen induced
95 modifications to RhoA (or RhoB or RhoC) to assemble an inflammasome (23). RhoA, RhoB and
96 RhoC appear to be functionally redundant in regulating pyrin activity (23) and will be referred to
97 as RhoA from here on. Inactivation of RhoA by the TcdB toxin of *Clostridioides difficile* or the
98 TecA effector of *Burkholderia cenocepacia* also triggers pyrin inflammasome assembly in
99 macrophages (23, 24). Pyrin is encoded by the *MEFV* gene (*Mefv* in mice) whose expression is
100 restricted to phagocytes such as neutrophils, monocytes and activated macrophages (25). Pyrin
101 is a TRIM protein and like other members of this family (26) human pyrin forms dimers via coiled
102 coil (CC) domains (27). Additionally, human pyrin has been shown to form trimers (28). Pyrin
103 potentially forms higher order oligomers (i.e. dimers of dimers), via B-box domains (21). It is not
104 known if murine pyrin forms oligomers. Structurally, murine and human pyrin are similar except
105 for their C-terminus. Murine pyrin lacks the B30.2 domain present in human pyrin (29). However,
106 the mechanism of pyrin regulation appears to be conserved in both species (30).

107 Negative regulation of pyrin occurs in a manner similar to the guard hypothesis observed in plants,
108 whereby a plant disease resistance PRR recognizes modifications to host proteins made by
109 pathogens and induces an innate response (31). More specifically, pyrin follows an indirect guard
110 hypothesis in which it does not directly interact with but is negatively regulated by RhoA (23).
111 Hence, pyrin acts as the guard of RhoA (guardee) to protect host cells from bacterial effectors or
112 toxins which target it. RhoA functions through a switch like mechanism between an “on” (Rho-
113 GTP) and “off” (Rho-GDP) state. RhoA has numerous roles in phagocytosis, cell cycle and
114 migration and is targeted by multiple bacterial pathogens (23, 32). Pyrin is negatively regulated
115 by serine phosphorylation, via the kinase PKN (also known as PRK), which is in turn is activated
116 by RhoA. PKN phosphorylates murine pyrin on serines 205 and 241 (S208 and S242 in human
117 pyrin) within 14-3-3-binding sites located in the linker region to negatively regulate pyrin (30, 33).
118 Mutational analysis of S205 and S241 by alanine substitution in ectopically expressed murine
119 pyrin indicates that loss of either site results in partial inflammasome activation and when both
120 sites are disrupted there is an additive effect (30). Similar studies of S208 and S242 in human
121 pyrin show that the inflammasome is activated when either site is substituted (33, 34). Moreover,
122 an S242R mutation in *MEFV* causes an autoinflammatory disease, PAAND, which leads to a
123 partially active form of pyrin and further underscores the importance of linker phosphorylation in
124 pyrin regulation (35). When pyrin is phosphorylated, the N-terminal pyrin domain (PYD) may be

125 sequestered, preventing interaction with ASC (21). RhoA inactivation removes the negative
126 regulation axis of pyrin, presumably resulting in dephosphorylation of S205/S208 and S241/S242
127 (21, 22, 30, 33). These findings lead to a model wherein when both serines in the pyrin linker are
128 dephosphorylated, 14-3-3 detaches, the PYD is exposed, and ASC and caspase-1 are recruited
129 to assemble inflammasomes (21, 30, 33). A limitation of this model is that no phosphoprotein
130 phosphatase (PPP) that dephosphorylates pyrin has been identified and the phosphorylation
131 status of pyrin oligomers is unknown.

132 Assembly of the pyrin inflammasome in phagocytes infected with WT *Yersinia* is blocked due to
133 the action of YopM (17, 18). YopM binds to and activates the protein PKN and a second kinase,
134 RSK (36). YopM hijacks PKN and RSK to keep pyrin phosphorylated (17, 21, 34). A *Yptb* Δ*yopM*
135 mutant is fully virulent in Mefv$^{-/-}$ mice, demonstrating that YopM promotes virulence by inhibiting
136 pyrin (17). The importance of pyrin in pathogenesis extends beyond *Yersinia, C. difficile* and *B.*
137 *cenocepacia* as numerous other bacteria including *Clostridium botulinum*, *Vibrio*
138 *parahaemolyticus* and *Histophilus somni* secrete toxins that trigger assembly of this
139 inflammasome in phagocytes (23).

140 Codon changes in the *MEFV* gene (e.g. M694V) that result in gain of function pyrin variants are
141 responsible for the monogenic human autoinflammatory disease Familial Mediterranean Fever
142 (FMF) (25, 34). FMF is characterized by recurrent episodes of fever and serositis and primarily
143 affects eastern Mediterranean populations (37). Magnotti et al demonstrated that pyrin
144 dephosphorylation was sufficient to promote inflammasome activation using PKN inhibitors on
145 monocytes from FMF patients, which implies that these patients have a lower threshold for pyrin
146 activation than healthy patients (38). It has been hypothesized that the high carrier frequency of
147 FMF in Mediterranean and Middle Eastern populations is the result of a selective advantage in
148 resistance to an unknown infection (34). Population genetic evidence is consistent with the idea
149 that plague selected for FMF mutations in Middle Eastern populations (34). In addition, infection
150 assays with human cells and mice provided evidence that pyrin FMF variants promote resistance
151 to *Y. pestis* (34). These findings underscore the importance of the pyrin inflammasome for human
152 health. Therefore, it is important to understand the dual role of pyrin in promoting immune
153 responses against pathogens and autoinflammation in FMF and a deeper understanding of pyrin
154 inflammasome regulation will aid in this goal.

155 Here we used primary murine macrophages and human THP-1 cells and primary monocytes from
156 FMF patients in conjunction with bacterial and chemical inhibitors, native PAGE, immunoblotting

157 with phospho-specific pyrin antibodies and siRNA knockdowns to determine if PPP activity is
158 required to dephosphorylate oligomeric pyrin and positively regulate inflammasome assembly in
159 response to inactivation of the RhoA-PKN axis.
160
161 RESULTS
162 **PPP activity is required for pyrin dephosphorylation and positive regulation of**
163 **inflammasome assembly**
164 Inactivation of RhoA removes negative regulation by PKN, however, a PPP is needed to positively
165 regulate pyrin by serine dephosphorylation. The PPP family consists of PP1, PP2A, PP2B (also
166 known as calcineurin or PP3), PP4, PP5, PP6, and PP7 (39). To test the role of PPPs in
167 dephosphorylation of pyrin LPS-primed bone marrow-derived macrophages (BMDMs) were
168 pretreated for 15 min with DMSO as a vehicle control or one the following inhibitors: calyculin A
169 (CA) at 10 nM and okadaic acid (OA) at 1000 nM, which at these concentrations inhibit PP1,
170 PP2A, PP4, PP5, and PP6 but not PP2B; OA at 100 nM to more specifically inhibit PP2A; and
171 1000nM of cyclosporin A (CSA) which inhibits PP2B. After the pretreatment the BMDMs were
172 maintained in the presence of DMSO or the inhibitors during intoxication for 90 min with *C. difficile*
173 TcdB, which glucosylates and inactivates RhoA (40), to trigger pyrin inflammasome assembly
174 (23). BMDM lysates were analyzed by immunoblotting with monoclonal antibodies specific for
175 total pyrin or phosphoserine 205 (PS205) (30) or actin as loading control. We were unable to
176 monitor PS241 in murine pyrin because the antibody reported to recognize this modification (30)
177 did not work in our hands for this purpose but did recognize human pyrin PS242 (see Fig.S3
178 below). We found that treatment of BMDMs with CA or 1000 nM OA prevented pyrin S205
179 dephosphorylation in response to TcdB intoxication (Fig.S1A). Results of ELISA on BMDM
180 supernatants showed that CA or 1000 nM OA also significantly reduced release of mature IL-1β
181 during TcdB intoxication (Fig.S1B). CSA treatment did not inhibit pyrin S205 dephosphorylation
182 or IL-1β release upon TcdB intoxication (Fig.S1) which indicates that PP2B does not regulate this
183 inflammasome. 100nM OA treatment was also ineffective (Fig.S1) but previous publications (41)
184 and subsequent experiments (see Fig.5 below) indicate that at this concentration longer
185 pretreatments are needed for the inhibitor to reach effective concentrations in cells. We noted that
186 CA and 1000nM OA in the absence or presence of TcdB caused an upshift in the positions of
187 pyrin bands on the immunoblots, but not a corresponding increase in PS205 signal (Fig.S1A).
188 This observation suggests that S205 is uniformly phosphorylated and a PPP constitutively
189 dephosphorylates pyrin at an additional site(s), possibly S241, and when this phosphatase is
190 inhibited, hyperphosphorylation by PKN results in reduced mobility of pyrin by SDS-PAGE. In

191 summary, these results suggest that a PPP other than PP2B is required to dephosphorylate pyrin
192 S205 and trigger assembly of the inflammasome in response to TcdB. In addition, a PPP may
193 act constitutively to dephosphorylate pyrin at another site(s).

194 We used CA treatment to determine if a PPP is important for YopE and YopT to trigger pyrin S205
195 dephosphorylation and inflammasome assembly in BMDMs infected with *Yptb.* BMDMs treated
196 with DMSO or CA as above were infected with a Δ*yopM* mutant to activate the pyrin
197 inflammasome. We also infected DMSO or CA-treated BMDMs with a Δ*yopK* mutant, which
198 triggers assembly of the NLRP3 inflammasome (and to a lesser degree the NLRC4
199 inflammasome) (19, 20), since there is evidence that PP2A is important for dephosphorylation
200 and activation of NLRP3 (42). Immunoblot and ELISA analysis of BMDMs pre-treated with CA
201 followed by Δ*yopM* infection showed that pyrin remained phosphorylated on S205 and there was
202 a significant decrease in IL-1β release (Fig. 1). Results of infection with Δ*yopK* also showed
203 reduced IL-1β release when the BMDMs were treated with CA, although the decrease was not
204 significant (Fig. 1B). Pyrin was not dephosphorylated on S205 in response to Δ*yopK* infection of
205 untreated BMDMs as expected (Fig. 1A). The finding that CA had a stronger inhibitory effect on
206 IL-1β secretion with Δ*yopM* as compared to Δ*yopK* infection (Fig. 1B) might reflect residual
207 NLRC4 inflammasome assembly triggered by the latter strain (19).

208 Similar results were obtained when CA was used to treat BMDMs infected with Δ*yopM Yptb*
209 strains expressing only active YopE ($yopT^{C139A}$) or YopT ($yopE^{R144A}$) (Fig. S2). In addition,
210 immunoblotting indicated that CA did not decrease steady state levels of pro-IL-1β (Fig. S2A).
211
212 *B. cenocepacia* infection of naive THP-1 cells has been shown to trigger assembly of the pyrin
213 inflammasome (43). To determine if PPP inhibition prevents dephosphorylation of human pyrin
214 we infected THP-1 cells with *B. cenocepacia* WT or Δ*tecA* strains in the absence or presence of
215 DMSO or CA. Lysates were immunoblotted with antibodies that recognize total pyrin, PS242,
216 pro-IL-1β or actin as loading control. *B. cenocepacia* infection triggered dephosphorylation of
217 S242 in a TecA-dependent manner in DMSO-treated THP-1 cells (Fig.S3). Interestingly, when
218 THP-1 cells were pretreated and maintained in the presence of CA, S242 became
219 hyperphosphorylated in both uninfected and infected conditions (Fig.S3), which was evident from
220 comparing the short and long exposures of the immunoblots. The hyperphosphorylation of pyrin
221 in the presence of CA in uninfected THP-1 cells suggests that a PPP is constitutively
222 counterbalancing PKN to keep S242 hypophosphorylated. CA treatment prevented infection-
223 induced production of pro-IL-1β as determined by immunoblotting (Fig.S3) and as a result the

224 impact of the inhibitor on release of mature IL-1β from the THP-1 cells could not be measured.
225 These data indicate that a PPP dephosphorylates pyrin S242 in response to inactivation of RhoA
226 by TecA in THP-1 cells, but it appears that a PPP is acting constitutively to keep most of the pyrin
227 in the cell dephosphorylated at this site prior to infection.
228
229 PKN inhibitors activate pyrin inflammasome assembly and pyroptosis in monocytes from FMF
230 patients with the M694V mutation (38). The effect of CA on release of IL-1β from FMF patient's
231 monocytes activated by treatment with the PKN inhibitor, UCN-01, was measured. Pre-treating
232 LPS-primed FMF monocytes with 40 nM CA followed by UCN-01 treatment significantly inhibited
233 IL-1β release as compared to UCN-01 treatment alone (Fig. 2). Moreover, CA treatment also
234 prevented UCN-01 mediated cell death as measured by propidium iodide influx in a human
235 monocytic cell line, U937, expressing the p.M694V *MEFV* variant (Fig.S4). Thus, in an FMF
236 context where the threshold of activation has been shown to be lower and relies on pyrin
237 dephosphorylation (38, 44), a PPP is constitutively countering the effect of the PKN kinases and
238 inhibition of PPP activity prevents inflammasome activation. Altogether these data replicate the
239 inhibitory effect of CA as seen on murine pyrin dephosphorylation and activation in BMDMs in
240 human cells.
241
242 **PPP activity regulates phosphorylation of oligomeric pyrin**
243 Although human pyrin has been shown to form trimers (28) the oligomeric status of murine pyrin
244 has not been investigated. In addition, it is not known if pyrin oligomers are differentially
245 phosphorylated or dephosphorylated. We used blue native PAGE (BN-PAGE) and
246 immunoblotting (45, 46) to examine the impact RhoA inactivation and PPP inhibition on
247 phosphorylation of oligomeric pyrin. To optimize the procedure, we first tested different non-ionic
248 detergent extraction conditions on untreated uninfected WT or *Mefv*$^{-/-}$ BMDMs. As shown in
249 Fig.S5, when extracts of untreated BMDMs were separated by BN-PAGE and immunoblotted for
250 total (A) or PS205 (B) pyrin, we detected oligomers of pyrin in WT but not *Mefv*$^{-/-}$ BMDMs.
251 Monomeric pyrin (~90 kDa) was not detected and based on the apparent molecular weight of the
252 oligomers we tentatively assigned them as dimer (~242 kDa) and higher-order oligomers (~480-
253 720 kDa). Thus, most of the pyrin in BMDMs is in a higher oligomeric form and phosphorylated
254 on S205. Recovery of total and PS205 pyrin was optimal using 0.5% or 1% digitonin (Fig.S5) and
255 1% was used going forward.
256

257 We next analyzed the phosphorylation and oligomeric status of pyrin in BMDMS infected with WT
258 or Δ*yopM Yptb* in the absence of CA using BN-PAGE and immunoblotting. As shown in Fig.3, the
259 total (A) and PS205 (B) pyrin oligomer signals decreased in BMDMs infected with Δ*yopM*, due to
260 increased insolubility of the dephosphorylated form of pyrin in non-ionic detergent (E) (22). This
261 insolubility issue prevented us from determining if the oligomeric state of pyrin is altered upon
262 dephosphorylation. In BMDMs treated with CA there was an upshift in the positions of the dimeric
263 and higher oligomeric forms under all conditions, most evident with the PS205 signal, and there
264 was no insolubility or dephosphorylation of pyrin in response to infection with Δ*yopM* (Fig.3CD).
265 In addition, in the presence of CA a very large mystery oligomer at ~1048 kDa was detected with
266 the PS205 signal under all conditions (Fig.3D). These results confirm the upshift in mobility due
267 to hyperphosphorylation of pyrin in the presence of CA seen in some SDS-PAGE immunoblots
268 (Fig.S1A). These data further suggest that hyperphosphorylation of pyrin increases
269 oligomerization.
270
271 **YopM interacts with oligomeric pyrin**
272 YopM can interact with pyrin as determined by co-immunoprecipitation (17, 18, 34). We
273 wondered if YopM interacts with the different oligomeric forms of YopM and if this interaction is
274 sensitive to PPP inhibition. To determine if YopM is associated with pyrin oligomers, samples
275 from untreated WT BMDMs left uninfected or infected with WT or Δ*yopM Yptb* were separated by
276 BN-PAGE and immunoblotted with antibody to YopM. We detected a YopM signal at the dimer
277 and higher-order oligomer positions in the WT but not in the Δ*yopM Yptb* samples (Fig.4A, lanes
278 2 and 3). We then repeated the experiments using WT BMDMs untreated or treated with CA or
279 untreated *Mefv*$^{-/-}$ BMDMs. In WT BMDMs there was a YopM signal corresponding to dimeric pyrin
280 in the DMSO and CA treated WT *Yptb* infected samples (Fig.4B, lanes 2 and 5). The higher order
281 oligomeric YopM signal around ~480kDa seen with DMSO treatment was not present in the CA
282 treated sample (Fig.4B, lane 5). In addition, there was a faint YopM signal around ~480kDa in
283 the *Mefv*$^{-/-}$ BMDMs infected with WT *Yptb* (Fig.4B, lane 8). Two dimensional BN-PAGE
284 immunoblot analysis of the DMSO treated and WT *Yptb* infected BMDMs sample showed a good
285 correspondence in the molecular weights of the YopM and oligomeric pyrin signals (Fig. 4C).
286 These results strongly indicate that YopM interacts with dimeric and higher order oligomers of
287 pyrin. Possible explanations for why YopM interaction with the higher order pyrin oligomer is
288 sensitive to PPP inhibition, and the presence of a weak YopM signal at this position in Mefv-/-
289 BMDMs are discussed below (see Discussion).
290

291 **The PP1 inhibitor tautomycetin does not prevent pyrin dephosphorylation or**
292 **inflammasome assembly**
293 To further delineate which PPP activities positively regulate pyrin, we used tautomycetin (TTN),
294 a more specific inhibitor of PP1 (47, 48). WT BMDMs were pretreated for 15 min and maintained
295 in DMSO or 1 or 2μM of TTN during infection with Δ*yopM Yptb.* We found that treatment of
296 BMDMs with TTN did not prevent pyrin PS205 dephosphorylation or IL-1β release in response to
297 infection with Δ*yopM Yptb* (Fig.S5). Longer pretreatment of BMDMs with 1μM TTN also did not
298 decrease IL-1β secretion upon Δ*yopM* infection (data not shown). Our combined results from
299 treatment of BMDMs with various phosphatase inhibitors suggest that a PPP other than PP1 and
300 PP2B is required to activate pyrin.
301
302 **Longer pretreatment with 100 nM OA reduces pyrin dephosphorylation and inflammasome**
303 **assembly**
304 As mentioned previously, OA penetration inside cells is slow and using a lower concentration of
305 OA generally requires longer pretreatment time to achieve sufficient inhibitory levels inside the
306 cell. In contrast CA readily partitions inside cells (41, 49, 50). We found that WT BMDMs
307 pretreated for 3hr and maintained with 100nM OA during infection with Δ*yopM Yptb* showed
308 reduced pyrin dephosphorylation (Fig. 5A) and a significant decrease in IL-1β release as
309 compared to the DMSO control (Fig.5B); whereas 15min pretreatment of BMDMs with 100nM OA
310 did not have such an inhibitory effect on pyrin activation (Fig. S1). Given the selectivity of 100 nM
311 OA to preferentially inhibit PP2A/PP4 over PP1/PP5 (50), these results suggest that PP2A or PP4
312 could be involved in positively regulating pyrin. Since most serine/threonine phosphatase
313 activities inside the cell are carried out PP1 and PP2A (39, 51) our results with TTN and longer
314 pretreatment with OA in BMDMs allude to a role for PP2A in positive regulation of pyrin activation.
315
316 **siRNA knockdown implicates PP2A in dephosphorylation of pyrin S205**
317 We next tested the effect of knocking down PP2A in BMDMs on pyrin inflammasome assembly.
318 PP2A has two catalytic subunit isoforms, alpha (PP2Aca) and beta (PP2Acb), which only differ in
319 a few amino acids from each other. We first tested two different siRNAs targeting the mRNA of
320 the alpha catalytic subunit of PP2A (42). The siRNAs (1000pmol) were electroporated into WT
321 BMDMs which were also LPS-primed. PKN1 siRNA was used as a positive control (17, 33). RT-
322 qPCR showed that there was significant and selective knock down of PP2Aca mRNA with both
323 siRNAs as compared to the positive control and PP2Acb analyzed in parallel (Fig. S6A). The
324 siRNA electroporations were then repeated and LPS-primed BMDMs were left uninfected or

325 infected with Δ*yopM Yptb.* Immunoblotting showed that there was full depletion of PKN1 with the
326 corresponding siRNA but only an apparent ~50% knock down of PP2A with the siRNAs #1 and
327 #2 (Fig.S6B). Since the PP2A antibody used detects both isoforms the remaining signal detected
328 could have corresponded to PP2Acb. Upon Δ*yopM* infection there was no inhibition of
329 dephosphorylation of pyrin at S205 with either PP2Aca siRNAs (Fig. S6B). However, PP2Aca #2
330 siRNA decreased IL-1β secretion (data not shown) which could indicate that this siRNA has an
331 off-target effect when used at the high concentration. A PP2Acb siRNA when tested by itself at
332 500pmol selectively knocked down the corresponding mRNA transcripts and did not decrease IL-
333 1β release as compared to the control (Fig.6A and Fig.S6C, respectively). We next tested the
334 effect of a combined PP2A alpha and beta catalytic subunit knock down. BMDMs were
335 electroporated with PKN1 or PP2Aca and PP2Acb siRNAs (500pmol each) and LPS primed as
336 before. RT-qPCR showed that there was a decrease in the mRNA transcripts of both PP2A
337 subunits (Fig.6A). Immunoblotting showed a greater depletion of PP2A protein as compared to
338 knocking down the alpha subunit alone (compare Fig.S6B and Fig.6B). Upon Δ*yopM* infection
339 PS205 pyrin was maintained and there was a significant decrease in IL-1β secretion with both
340 siRNA combinations tested (Fig.6B and C, respectively). Together, these results implicate PP2A
341 alpha and beta subunits as acting redundantly to dephosphorylate pyrin S205.
342
343
344 DISCUSSION
345
346 In this study, we aimed to understand if a PPP activity is important for positive regulation of
347 inflammasome assembly by oligomeric pyrin. There are seven different PPPs in the mammalian
348 cell: PP1, PP2A, PP2B (PP3), PP4, PP5, PP6 and PP7. In the human genome there are ~428
349 Ser/Thr kinases but only ~30 Ser/Thr phosphatases (51). The remarkable diversity of PPP
350 substrates, substrate recognition and cellular localization is achieved by the association of
351 catalytic subunits with non-catalytic subunits to form multimeric holoenzymes (39). The active
352 sites of these phosphatases share 100% similarity, and most phosphatase inhibitors which bind
353 to the PPP active sites are broadly specific for this reason.
354
355 CA is a relatively non-specific and hydrophobic PPP inhibitor. It can easily partition through cell
356 membranes and potently inhibits most PPPs except for PP2B and PP7 (50). CA was found to
357 inhibit both murine and human pyrin inflammasome activation. Using 10nM CA we obtained
358 evidence that a PPP activity is important for pyrin S205 dephosphorylation and inflammasome

359 assembly in BMDMs in response to RhoA inactivation by TcdB or YopE/T during Δ*yopM Yptb*
360 infection. The same CA treatment also prevented TecA-dependent dephosphorylation of pyrin
361 S242 in THP-1 cells infected with *B. cenocepacia.* It has been shown previously in mouse
362 peritoneal macrophages that 50nM CA prevented activation of NLRP3, AIM2 and NLRC4
363 inflammasomes, indicating that PPP activity can be important for inflammasome activation in
364 general, and is perhaps acting at a latter step (52). We observed that 10nM CA prevented
365 infection-induced pro-IL-1β synthesis in THP-1 cells infected with *B. cenocepacia* illustrating that
366 results with this inhibitor need to be carefully controlled and interpreted since it can block multiple
367 steps in an inflammasome pathway. Moreover, 40 nM CA was also found to reverse the effect of
368 a PKN inhibitor and potently inhibit pyrin activation in FMF patient monocytes. These cells have
369 previously been demonstrated to exhibit a lower activation threshold for inflammasome activation
370 as compared to monocytes from healthy donors, and pyrin dephosphorylation has been to shown
371 to be sufficient to trigger inflammasome assembly in FMF monocytes (37, 38). It is possible that
372 in the FMF disease context, a balance between the PKN kinases and a PPP regulates
373 inflammasome assembly and inhibition of either shifts the equilibrium in favor of the other protein.
374 Results from our experiments with treatment of BMDMs with CA and Δ*yopK Yptb* mutant infection
375 showed that there was a non-significant decrease in IL-1β release which can be attributed to
376 inhibition of NLRP3 but not of the NLRC4 inflammasome. Luheshi et al used a higher CA
377 concentration of 50nM (52) which could explain why we didn't observe inhibition of NLRC4
378 inflammasome in response to Δ*yopK* infection with 10nM CA treatment.
379
380 We were also able to show using BN-PAGE that murine pyrin forms oligomers consisting of
381 dimers and higher order oligomers that are phosphorylated on S205 when pyrin is inactive. Due
382 to the insolubility of active pyrin in non-ionic detergent we were unable to determine if
383 dephosphorylation changes the oligomeric status of pyrin. However, PPP inhibition with CA
384 resulted in the appearance of a very high molecular weight mystery oligomer which indicates that
385 phosphorylation increases oligomerization of pyrin. Pyrin belongs to the TRIM family of proteins
386 and Trim5α which is involved in HIV viral capsid recognition is known to form dimers and higher
387 order lattices consisting of dimers of dimers or trimers of dimers (26). The higher order murine
388 pyrin oligomers (~480-720kDa) that we observe on BN-PAGE immunoblots could represent
389 dimers of dimers or trimers of dimers similar to those formed by Trim5α. It has been previously
390 shown through crosslinking studies in THP-1 cell lysates that human pyrin can form trimers which
391 is mediated through its coiled coil domains (28). In the same study it was also shown that the B-
392 box domain of human pyrin interacts with the N-terminal pyrin domain to sequester it and prevent

393 interaction with ASC (28). However, Weinert et al reported that a truncated version of human pyrin
394 forms an antiparallel dimer in vitro through interaction of coiled coil domains (27). These
395 discrepancies in trimer vs dimer formation by human pyrin could be attributed to experimental and
396 technical differences. It is expected that regulation of human and murine pyrin by oligomerization
397 would be conserved but due to structural differences, it is possible that murine pyrin forms dimers
398 and human pyrin forms trimers through their respective coiled coil domains. To rule out technical
399 differences it would be informative to investigate oligomerization of human pyrin by BN-PAGE
400 instead of crosslinking. The phosphorylation status of human pyrin oligomers should also be
401 determined.
402
403 CA treatment resulted in an upshift in molecular weights of PS205 and total murine pyrin bands
404 in all conditions on BN-PAGE immunoblots, as wells as on some SDS-PAGE immunoblots. In
405 addition, CA treatment of THP-1 cells resulted in hyperphosphorylation of S242 in human pyrin.
406 This indicates that a PPP acts constitutively on the second linker site in pyrin to dephosphorylate
407 it and when this PPP is inhibited the second serine becomes hyperphosphorylated. These results
408 suggest that one of the linker sites can be hypophosphorylated yet pyrin remains inactive. This
409 finding is surprising given the data that phosphorylation of the second linker site is critical for
410 negative regulation of pyrin, based on alanine substitution of this residue in ectopically expressed
411 pyrin variants (33, 34). In addition, the S242R substitution causes PAAND in which the pyrin
412 variant is considered constitutively active (35). Pull down experiments in this study also showed
413 that 14-3-3 proteins are not bound to the S242R variant and that pyrin is dephosphorylated (35).
414 Jeru et al. showed previously that a S208A pyrin variant has reduced 14-3-3 binding while the
415 S242A mutant abolishes 14-3-3 binding (53). This suggested that 14-3-3 binding could follow a
416 gatekeeper hypothesis in which PS242 is the dominant site which promotes 14-3-3 binding and
417 PS208 is a secondary site (53). These findings may indicate that hypophosphorylation of the
418 second linker site is sufficient to keep pyrin oligomers inactive. This could facilitate fast
419 dephosphorylation of the hypophosphorylated second sites, resulting in rapid activation of pyrin
420 in response to RhoA inactivation by pathogens. A caveat of this concept is our limitation of not
421 being able to measure the phosphorylation status of S241 in murine pyrin under the conditions
422 used.
423
424 We were also able to use one and 2D BN-PAGE and immunoblotting to detect interaction of
425 murine pyrin with YopM during WT *Yptb* infection of BMDMs and found that this interaction was
426 sensitive to PPP inhibition. The fact that YopM targets the oligomers argues that they are poised

427 to become activated upon dephosphorylation. We hypothesize that the faint YopM signal on BN-
428 PAGE immunoblots from the *Mefv*$^{-/-}$ BMDMs infected with WT *Yptb* could result from self-
429 oligomerization of the YopM protein. The YopM protein from *Y. pestis* is known to form tetramers
430 in vitro (36, 54), so it is conceivable that the *Yptb* YopM protein can form higher order oligomers
431 on its own in *Mefv*$^{-/-}$ BMDMs. One explanation for the selective loss of the YopM signal at the
432 position of the higher order oligomers from the CA-treated and WT *Yptb*-infected samples is that
433 the affinity of YopM binding to pyrin is reduced by hyperphosphorylation.
434
435 OA in comparison to CA has a greater inhibitory constant to bind to the catalytic subunit of PP2A
436 than of PP1 and is reported to enter cells slowly (50, 55). Our results indicated that 15min
437 pretreatment with 1000nM OA is sufficient to inhibit S205 pyrin dephosphorylation and IL-1β
438 release in BMDMs upon RhoA inactivation. Stutz et al reported that PP2A is important for NLRP3
439 activation through dephosphorylation using the same conditions and concentration of OA (42).
440 We only observed a reduction in S205 dephosphorylation and a significant decrease in IL-1β
441 secretion in response to Δ*yopM* infection when BMDMs were pretreated with 100nM OA for 3hr
442 but not for 15min, which can be explained by the slow entry of the inhibitor. We hypothesize from
443 these results that PP2A plays a role in dephosphorylation of S205 and positive regulation of the
444 pyrin inflammasome in BMDMs.
445
446 PP2A, along with PP1, carry out most serine/threonine dephosphorylation events in cells and
447 partake in many essential activities for the cell (39). PP2A is abundantly present in cells and forms
448 heterotrimers consisting of a catalytic subunit, a scaffolding A subunit, and a regulatory B subunit
449 (39). There are two isoforms of the catalytic and scaffolding subunits, and four isoforms of the
450 regulatory subunits, which account for the diverse activities and substrates regulated by PP2A
451 (51). Since it is an essential protein for the cell and very likely has a long half-life which explains
452 why we were unable to fully deplete it in the cell. The alpha and beta catalytic subunit of PP2A
453 only differ by a few amino acids and PP2Aca is more abundantly present in cells than PP2Acb.
454 Our results indicated that siRNAs targeting PP2Aca did not reduce S205 pyrin dephosphorylation
455 in BMDMs infected with Δ*yopM*. However, a combined knock down of both catalytic subunits of
456 PP2A showed that S205 pyrin phosphorylation was maintained and there was a significant
457 decrease in IL-1β secretion upon Δ*yopM* infection. These results indicate that the two catalytic
458 subunits of PP2A act redundantly to dephosphorylate the pyrin linker. This is distinct from the
459 case of NLRP3 where knockdown of the alpha catalytic subunit of PP2A alone was sufficient to
460 prevent assembly of the inflammasome (42). To confirm our results, additional siRNAs targeting

461 the alpha and beta catalytic subunit of PP2A should be tested. In addition, the impact of PP2A
462 knockdowns on PS241 in murine pyrin and PS208/242 in human pyrin needs to be investigated.
463 Furthermore, in a broader disease context, the effect of PP2A knockdown on FMF pyrin activation
464 should also be explored because it may offer insights for new therapeutic strategies.
465
466 PPPs recognize and bind to regulatory proteins or to substrates via short linear motifs (SLiMs)
467 (39). For example, the B56 regulatory subunit of PP2A binds through LxxIxE motifs to its
468 substrates (39). Interestingly, murine pyrin contains two LxxIxE motifs in the coiled-coil domain
469 and human pyrin has one LxxIxE motif in the linker. Since both murine and human pyrin have a
470 PP2A-B56 regulatory motif it is possible that PP2A regulates both forms through a conserved
471 mechanism. This could be tested by inactivation of the SLiM motifs in murine and human pyrin.
472 We have not ruled out the possible roles of other PPPs in pyrin dephosphorylation and
473 inflammasome assembly and additional approaches will likely be needed to address this
474 possibility. Finally, it remains to be determined if the activity of PP2A is upregulated upon RhoA
475 inactivation, or these enzymes simply constitutively counterbalance PKN. In the case of PP2A
476 activating NLRP3 by dephosphorylation (42), there is evidence that Bruton tyrosine kinase
477 negatively regulates PP2A by phosphorylation of tyrosine 307 (56). It is theoretically possible that
478 PKN could negatively regulate PPP activities by phosphorylation and additional experiments are
479 needed to address this possibility.
480
481 MATERIALS AND METHODS
482
483 **Bacterial strains.** *Y. pseudotuberculosis* (*Yptb*) 32777 (serogroup O1) strains used in this study
484 are as follows: wild-type (57), Δ*yopM* (58), Δ*yopK* (59), *yopE*^{R144A}*ΔyopM* and *yopT*^{C139A}*ΔyopM*
485 (17). *Yptb* was grown at 28°C on Luria broth (LB) agar plates or with shaking in LB broth,
486 supplemented with antibiotics when necessary. The *B. cenocepacia* strains used were AU1054
487 (WT) and Δ*tecA* mutant (60). *B. cenocepacia* was grown at 37°C on LB agar plates or with
488 shaking in LB broth.
489
490 **Bone marrow isolation and cell culture conditions.** Bone marrow derived macrophages
491 (BMDMs) were obtained from femurs of 8-week-old WT C57BL/6 mice (Jackson Laboratories)
492 and/or *Mefv*$^{-/-}$ mice (61) as previously described (19). Cells were grown at 37°C in a humidified
493 incubator in macrophage growth media (MGM) made up of Dulbecco's modified Eagle Medium
494 (DMEM) plus GlutaMAX (Gibco) containing 10% heat inactivated fetal bovine serum (FBS) (GE

495 Health Care), 10% L929 cell-conditioned medium, 1 mM sodium pyruvate (Gibco), 10 mM HEPES
496 (Gibco) for a week. On day 7 differentiated macrophages were divided into six-well plates at a
497 density of 0.8×10^6 cells/well in a total volume of 3 ml in MGM diluted to contain 10% L929 cell-
498 conditioned medium (MGM 10/10) and primed for ~18hrs with 100 ng/ml O26:B6 *Escherichia coli*
499 LPS (Sigma).
500
501 **BMDM infection, intoxication, and inhibitor treatments.** For BMDM infections, *Yptb* strains
502 were grown overnight in LB at 28°C. The following day, cultures were diluted 1:40 in LB containing
503 20 mM sodium oxalate and 20 mM MgCl2 and grown at 28°C for 1 hr, then shifted to 37°C for 2
504 hr. Cultures were centrifuged and the bacterial pellets were resuspended in phosphate-buffered
505 saline (PBS). Bacterial suspensions were then diluted in media lacking FBS and containing 10%
506 L929 cell-conditioned medium (MGM 0/10). LPS-primed BMDMs were washed once with PBS
507 and left uninfected or infected in MGM 0/10 with *Yptb* strains cultured under conditions as
508 described above at an MOI of 30. Plates were centrifuged for 5 min at 106xg to facilitate contact
509 between *Yptb* and macrophages. Plates were then incubated at 37°C in 5% CO_2. In experiments
510 where the glucosyltransferase toxin TcdB from *Clostridium difficile* (List Biological Laboratories,
511 Inc.) was used as a positive control for pyrin inflammasome activation, BMDMs were intoxicated
512 with TcdB at a concentration of 0.1 µg/ml for 90min in MGM 0/10 media.
513
514 In experiments where phosphatase inhibitors were used and BMDMs were pre-treated for 15min
515 with either 1.4mM DMSO as vehicle control or calyculin A (10nM diluted from 100µM stock, LC
516 Laboratories), cyclosporin A (1µM diluted from 1mM stock, Sigma), okadaic acid (100nM or 1µM
517 diluted from 1mM stock, Tocris), or tautomycetin (1µM or 2µM diluted from 1mM stock, Tocris) in
518 MGM 0/10. MGM 10/10 was used for BMDMs pre-treated for 3hr with 100nM okadaic acid. For
519 infection following pre-treatment, MGM 0/10 media containing bacteria and DMSO or the
520 respective phosphatase inhibitors was added to the BMDMs, followed by centrifugation and
521 incubation as above. Post-infection, cell supernatants were collected and processed for IL-1β
522 detection by ELISA and cell lysates were prepared and processed for immunoblot analysis (see
523 below).
524
525 **THP-1 cells, infection, and inhibitor treatment.** THP-1 cells (ATCC TIB-202) were grown in
526 filter sterilized RPMI 1640 media (Cat. No 30-2001) containing 10% heat inactivated fetal bovine
527 serum and 0.05 mM 2-mercaptoethanol in $25cm^2$ flasks. When confluent the THP-1 cells were
528 expanded in $75cm^2$ flasks. No cells were used that were passaged more than 30 times. For

529 infections, THP-1 cells were seeded at a density of 0.8×10^6 cells per well in 1.5ml of media in 6-
530 well plates and pretreated with 1.4mM DMSO vehicle control or 10nM calyculin A for 15 min.
531 Overnight (16-hour) cultures of *B. cenocepacia* were subcultured 1:100 in fresh LB on infection
532 day and shaken at 37°C until the cultures reached mid-log phase (OD_{600} = 0.300). Cultures were
533 then centrifuged, the LB was removed, and the bacterial pellets were resuspended in PBS and
534 then diluted to an MOI of 20 in warmed RPMI 1640 media without FBS and containing DMSO or
535 calyculin A. 1.5ml of supplemented media was added to each well and mixed by pipetting gently
536 up and down. Following incubation for 3 hours at 37°C, the contents of each well was collected
537 and centrifuged for 10 minutes at 14,000rpm and 4°C. The cell pellet was collected and lysed for
538 immunoblot analysis as described below.
539
540 **FMF monocytes and inhibitor treatment.** Primary monocytes purified as described (38) from
541 three FMF patients carrying the p.M694V/p.M694V mutation were seeded into 96-well plates at
542 5×10^3 cells/well, in RPMI 1640, GlutaMAX medium (Thermo Fisher Scientific) supplemented with
543 10% fetal calf serum (Lonza). Cells were incubated for 2.5h in the presence of LPS (10 ng/ml,
544 InvivoGen) and, when indicated, pre-treated for 30 min with calyculin A (40nM, Sigma 208851),
545 followed by treatment with UCN-01 (12.5 µM, Sigma) for 90 minutes. Following the incubation,
546 cells were centrifuged, and supernatants were collected.
547
548 **U937 cell line and genetic manipulation.** The protocol for genetically manipulating the human
549 myeloid cell line U937 (CelluloNet, Lyon, France) was followed as described previously in (38).
550 Cells were grown in RPMI 1640 medium with glutaMAX-I supplemented with 10% (vol/vol) FCS,
551 2 mM L-glutamine, 100 IU/ml penicillin, and 100 µg/ml streptomycin (Thermo Fisher Scientific).
552 *MEFV*^{KO} cell lines generated by CRISPR/Cas9-mediated gene invalidations have been previously
553 described (38, 62). p.M694V *MEFV* was cloned into the GFP-expressing plasmid pINDUCER21
554 (63) under the control of a doxycycline-inducible promoter through the pENTR1A (Invitrogen)
555 vector using a synthetic DNA fragment (GeneArt) encoding the p.M694V Pyrin protein. Lentiviral
556 particles were produced in 293T cells using pMD2.G and psPAX2 (from Didier Trono, Addgene
557 plasmids #12259 and #12260), and pINDUCER-21 p.M694V Pyrin. U937 *MEFV*^{KO} cell lines were
558 transduced by spinoculation and sorted at day 7 post-transduction based on GFP expression on
559 an Aria cell sorter. Pyrin expression was induced by treatment with doxycycline (1 µg/ml) for 16 h
560 before stimulation.
561

562 **Real-time cell death assay.** U937 *MEFV*^{KO} cells expressing the p.M694V *MEFV* variant were
563 seeded at 5×10^4 per wells before stimulation in black 96-well plate (Costar, Corning) with
564 propidium iodide (PI, Sigma) at 5 µg/ml. Three technical replicates per conditions were done.
565 Cells were pre-treated with calyculin A (Sigma, 208851) at 40 nM for 30 min and then treated with
566 UCN-01 (Sigma, U6508) at 12.5 µM. Real-time PI incorporation was measured every 5 min for 6
567 hours post-UCN-01 addition on a fluorimeter (Tecan) using the following wavelengths: excitation
568 535 nm (bandwidth 15 nm) and emission 635 nm (bandwidth 15 nm) (64, 65). Cell death was
569 normalized (previously described, (38)) using PI incorporation in monocytes treated with 1%
570 Triton X-100 for 15 min (=100% cell death). As a further correction, the first time point of the
571 kinetics was set to 0.
572
573 **Protein analysis by SDS-PAGE and immunoblotting.** To obtain cell lysates, BMDMs and THP-
574 1 cells were lysed in mammalian protein extraction reagent (MPER, Thermo Scientific) along with
575 cOmplete Mini (Roche) protease inhibitor and PhosSTOP (Roche) phosphatase inhibitor. The
576 lysis buffer for THP-1 cells was supplemented with 10 nM calyculin A. Protein concentration was
577 normalized after measurement with a bichinonic acid assay (BCA, Thermo Fisher Scientific) and
578 3-10µg of total protein cell lysates was run on 4 to 12% NuPAGE Bis-Tris SDS-PAGE gels
579 (Invitrogen by ThermoFisher Scientific) and transferred to polyvinylidene difluoride membranes
580 (ThermoFisher Scientific) using an iBlot 2 gel transfer device (Life Technologies). Membranes
581 were blocked in 5% nonfat dairy milk (add company) and incubated with primary antibodies
582 overnight. Primary antibodies used in this paper were: rabbit-anti-mouse monoclonal total pyrin
583 antibody (1:1000 dilution, ab195975; abcam), rabbit-anti-mouse pyrin polyclonal (1:1000 dilution,
584 (61)), rabbit-anti-mouse phospho-serine 205 monoclonal antibody (1:1000 dilution, ab201784;
585 abcam), rabbit-anti-mouse phospho-serine 241 monoclonal antibody (1:1000 dilution, ab201784;
586 abcam), rabbit-anti-mouse/human IL-1β (1:1000 dilution, number 12242; Cell Signaling), rabbit-
587 anti-mouse/human polyclonal β-actin (1:1000 dilution, number 4967; Cell Signaling), mouse-anti-
588 mouse/human/rat monoclonal PP1a (1:1000 dilution, number MA5-17239, ThermoFisher
589 Scientific), rabbit-anti-*Y.pestis* polyclonal YopM (1:1000 dilution, provided by Susan Straley),
590 mouse-anti-mouse monoclonal PKN (1:1000 dilution, number 393344, Santa Cruz
591 Biotechnology), rabbit-anti-mouse monoclonal PP2A (1:1000 dilution, #2038, Cell Signaling), and
592 rabbit-anti-mouse GSDMD (1:1000 dilution, ab209845, Abcam). Horseradish peroxidase-
593 conjugated anti-rabbit or mouse antibody (Jackson Laboratory) were used as secondary
594 antibodies. Protein bands bound by antibodies were visualized using chemiluminescent detection
595 reagent (GE Healthcare) on an iBright FL1500 (ThermoFisher Scientific). Immunoblot

596 quantification was performed using the iBright analysis software and 'local corrected volume' in
597 the software was used to represent signal intensity for a band where indicated.
598
599 **Protein analysis by blue native (BN)-PAGE and immunoblotting.** BN-PAGE immunoblotting
600 was performed as described by Kofoed and Vance (46). All reagents for this procedure were
601 obtained from Invitrogen except as stated. BMDMs were lysed in non-denaturing 1X Native-PAGE
602 Novex sample buffer with the indicated concentrations of either digitonin (5% stock) or DDM (10%
603 stock), MPER (Thermo Scientific) or RIPA lysis or extraction buffer (Thermo Scientific), along with
604 cOmplete Mini (Roche) protease inhibitor and PhosSTOP (Roche) phosphatase inhibitor. Lysates
605 were centrifuged at 20,817xg for 10min to obtain soluble and insoluble fractions. In some
606 experiments the insoluble fractions of 1% digitonin lysates were analyzed by SDS-PASGE and
607 immunoblotting as described above. Protein concentrations of soluble fractions were normalized
608 after measurement with a bichinonic acid assay (BCA, Thermo Fisher Scientific) and 10µg or
609 more of total protein cell lysates was mixed with NativePAGE G-250 additive and loaded on 4-
610 16% NativePAGE Novex 3–12 % Bis-Tris gels. NativeMark unstained protein standard was used
611 for molecular weight standard visualization. XCell SureLock Mini-Cell was used for running the
612 gels. Samples were run at room temperature (RT) at constant 150V for 105-120min using pre-
613 chilled buffers. Dark blue cathode buffer (10ml NativePAGE running buffer, 10ml NativePAGE
614 cathode additive, 180ml deinonized water) was used for the inner chamber 19ntil samples had
615 run up to 1/3rd of the gel length after which the buffer was replaced with light blue buffer (10ml
616 NativePAGE running buffer, 1ml NativePAGE cathode additive, 189ml deinonized water) for the
617 remainder of the run. The outer chamber was filled with NativePAGE running buffer. Gels were
618 soaked in 2X NuPAGE transfer buffer (Invitrogen) for 15min at shaking at room temperature.
619 Proteins were transferred to polyvinylidene difluoride membranes (ThermoFisher Scientific) using
620 the template program P3 (20V constant, 7min) and an iBlot 2 gel transfer device (Life
621 Technologies). Post transfer membranes were incubated in 8% acetic acid for 15min with shaking,
622 followed by ponceau S staining for 5min. Membranes were washed with distilled water for 5min
623 to remove excess ponceau S stain then air-dried, reactivated by immersion in methanol, followed
624 by blocking in 5% non-fat dry milk. Primary and secondary antibodies used are mentioned above.
625
626 **Protein analysis by two-dimensional blue native (BN)-PAGE and immunoblotting.** The
627 procedures used followed a previously described protocol (46). Samples were prepared as
628 described above and separated on NativePAGE Novex 3–12 % Bis-Tris gels. Gel slices
629 containing samples of interest were excised, trimmed to be 3mm shorter in length than the size

630 of the 2D well in NuPAGE 4–12 % Bis-Tris 2D Gels, then submerged and shaken at RT in 1X
631 NuPAGE sample buffer containing 0.1M DTT. Gel slices wwere then microwaved for ~20sec to
632 denature proteins followed by cooling with shaking at 10min at RT. Slices were then fitted into the
633 2D well and SDS-PAGE immunoblotting was performed as described above.
634
635 **siRNA knock-down.** siRNAs targeting *Pkn1* (s115927), *PP2Aca* (#1: s72067, #2: s72066) and
636 *PP2Acb* (s72069) were obtained from Invitrogen. For siRNA gene knock-down experiments,
637 400pmol of *Pkn1*,1000pmol of *PP2Aca* siRNAs, and for combined PP2Ac knock down, 500pmol
638 each of PP2Aca siRNA and PP2Acb siRNA were transfected into BMDMs (1×10^6 cells) by
639 electroporation using the Neon Transfection System (Invitrogen) and electrical parameters of
640 1400V, 20ms and 2 pulses. BMDMs were then replated in 6-well plates and grown in MGM 10/10
641 media. 24hr following transfection, media was changed to fresh MGM 10/10 and LPS was added
642 for overnight incubation. 48hr following transfection BMDMs were infected with Δ*yopM Yptb* as
643 described above.
644
645 **Quantitative real-time PCR (RT-qPCR).** At 48hr following transfection, uninfected BMDMs were
646 lysed with trizol reagent (Invitrogen) to isolate RNA according to the manufacturer's instructions.
647 500-1000ng of RNA was used to make cDNA using SuperScript IV First-Strand Synthesis System
648 (Invitrogen). Approximately ~5ng of cDNA was quantified using PowerUp SYBR Green Master
649 Mix (Invitrogen) in the (add machine name). Primer specificity was checked by melt-curve
650 analysis. Expression of target genes was normalized to the expression of the housekeeping gene
651 Hprt. For fold change analysis data was transformed using the 'relative standard curve method
652 and comparative threshold cycle (Ct) method (ΔΔCt)' as described by Applied Biosystems.
653 Published primer sequences were used for qPCR analysis (42) and the sequences are: Hprt,
654 forward 5′-TGAAGT ACTCATTATAGTCAAGGGCA-3′ and reverse 5′-CTG
655 GTGAAAAGGACCTCTCG-3′; Ppp2ca, forward 5′-TCTTCCTCTCACTGCCTTGGT-3′ and
656 reverse 5′-CAG CAAGTCACACATTGGACCC-3′; Ppp2cb, forward 5′-
657 AAGGCGTTCACCAAGGAGCT-3′ and reverse 5′- ACAGCGGACCTCTTGCACAT-3′.
658
659 **IL-1β quantification.** IL-1β in BMDM supernatants was quantified using a murine (MLB00C; R&D
660 Systems) and human (R&D Systems) ELISA kit by following the manufacturer's instructions.
661

662 **Statistical analysis.** GraphPad Prism was used to perform statistical analyses. IL-1β ELISA data
663 were analyzed by one-way or two-way analysis of variance (ANOVA; Bonferroni multiple-
664 comparison test), or by Krukal-Wallis test (Dunn's multiple comparison test) as specified.
665
666 **Ethics statement.** The study was approved by the French Comité de Protection des Personnes
667 (CPP,#L16-189) and by the French Comité Consultatif sur le Traitement de l'Information en
668 matière de Recherche dans le domaine de la Santé (CCTIRS, #16.864). The authors observed a
669 strict accordance to the Helsinki Declaration guidelines. All FMF patients fulfilled the Tel
670 Hashomer criteria for FMF and were homzygous for the p.M694V mutation.
671
672 **Acknowledgments.** We thank Isha Nasa for help in providing advice on the phosphatase
673 inhibitors used in Fig. S1. We would also like to thank members of the Bliska lab for providing
674 helpful suggestions towards this project. Research reported in this publication was supported by
675 the National Institute of Allergy and Infectious Diseases of the National Institutes of Health under
676 Award Number R01AI099222 (JBB).
677

678 **FIGURES**

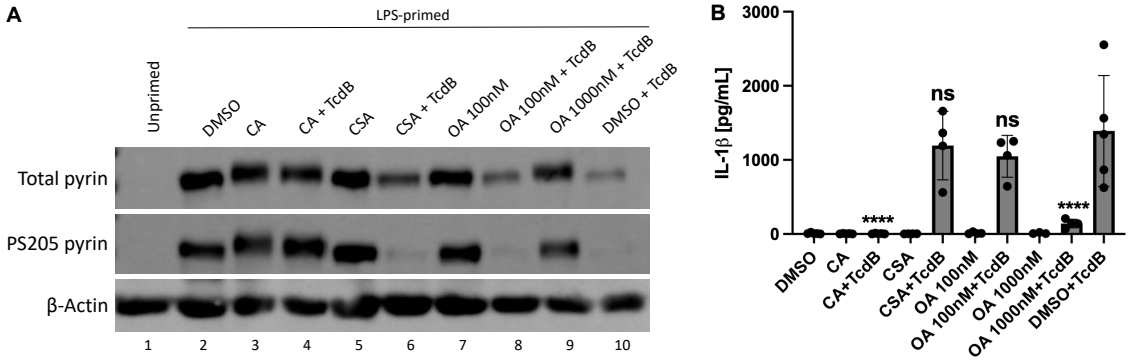

679
680 Fig.S1. PPP inhibition with CA and OA prevents pyrin S205 dephosphorylation and reduces IL-
681 1β release in BMDMs intoxicated with TcdB. LPS-primed BMDMs were pretreated for 15mins
682 and maintained with either 10nM calyculin A (CA), 100nM okadaic acid (OA), 1000nM OA or
683 1000nM cyclosporin A (CSA), and left unintoxicated or intoxicated with 0.1μg/mL of TcdB for 90
684 mins. Unprimed BMDMs or treatment with vehicle DMSO were used as controls. A) Immunoblot
685 analysis of total and PS205 pyrin in BMDM lysates. Actin was used as a loading control. B)
686 Mature IL-1β in supernatants as quantified by ELISA. Two-way ANOVA with Bonferroni post hoc
687 correction was applied to calculate significance and p-values as compared to DMSO+TcdB are
688 indicated. P-value<0.05 was considered significant; <0.0001 (****); not significant (ns). Each data
689 group is presented as an average (error bars are standard deviation) of at least 3 independent
690 experiments.
691
692
693
694
695
696
697
698
699
700

701

702

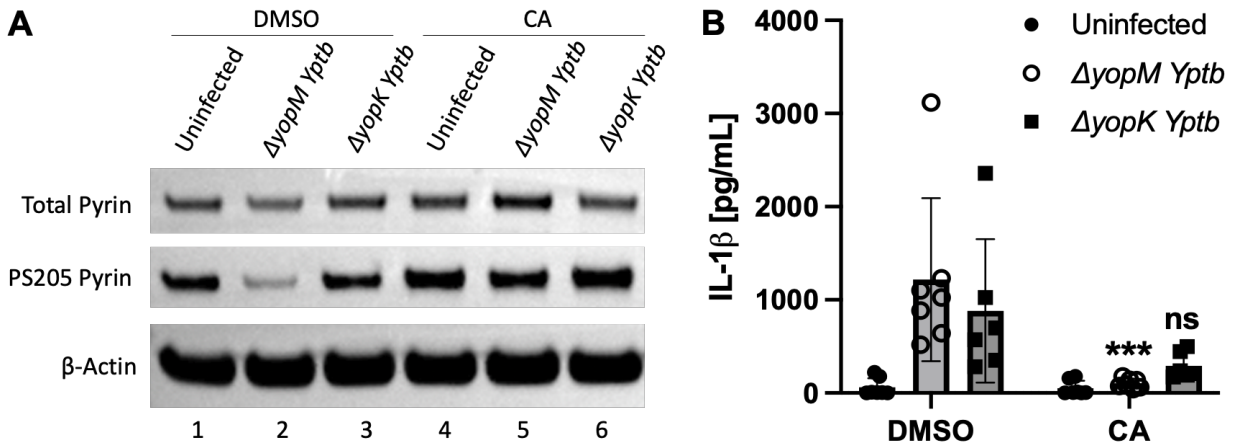

Fig.1. PPP inhibition with CA reduces pyrin dephosphorylation and IL-1β release in BMDMs infected with Δ*yopM Yptb.* LPS-primed BMDMs were pre-treated for 15mins and maintained with either DMSO or 10nM CA, and infected with the Δ*yopM* or Δ*yopK* strain at an MOI of 30 for 90 mins. Treated uninfected BMDMs were analyzed in parallel. A) Immunoblot analysis of PS205 and total pyrin in BMDM lysates. Actin was used as a loading control. B) Mature IL-1β in supernatants as quantified by ELISA. Two-way ANOVA with Bonferroni post hoc correction was applied to calculate significance and p-values of each treatment as compared to its corresponding DMSO treated infected strain is indicated. P-value<0.05 was considered significant; <0.001 (***); not significant (ns). Each data group is presented as an average (error bars are standard deviation) of at least 3 independent experiments.

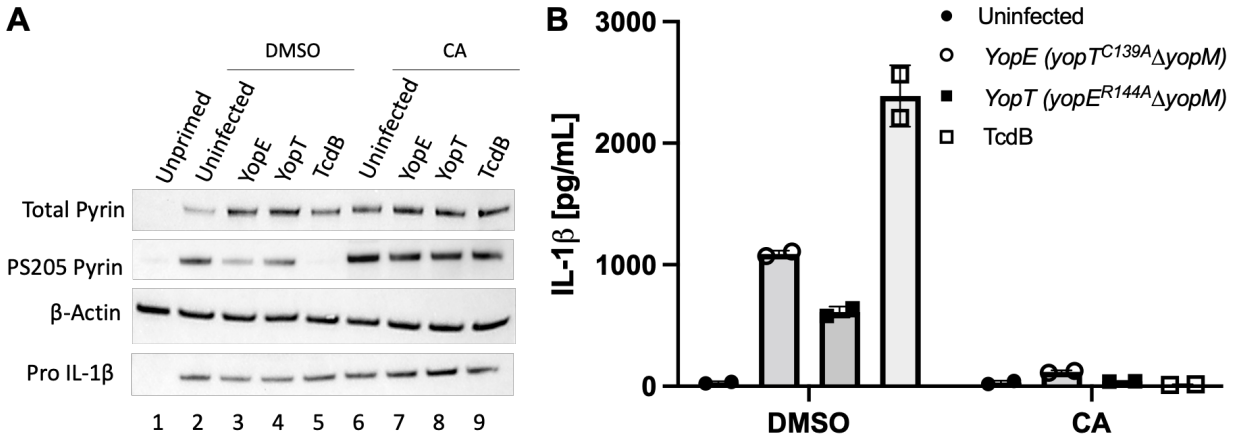

Fig.S2. PPP inhibition with CA reduces pyrin dephosphorylation and IL-1β release in BMDMs infected with Δ*yopM Yptb* strains expressing only active YopE or YopT. LPS-primed BMDMs were pre-treated for 15min and maintained with either DMSO or 10nM CA, and either infected with the Δ*yopM Yptb* YopE (*yopT*^{C139A}) or YopT (*yopE*^{R144A}) strains at an MOI of 30 or intoxicated with 0.1μg/mL of TcdB for 90 mins. Unprimed and uninfected BMDMs were analyzed in parallel as controls. A) Immunoblot analysis of PS205 and total pyrin and pro-IL-1β in BMDM lysates. Actin was used as a loading control. B) Mature IL-1β in supernatants as quantified by ELISA. Each data group is presented as an average (error bars are standard deviation) of two technical replicates.

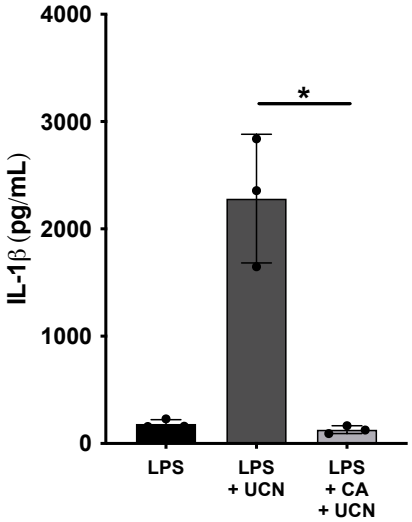

Fig. 2. CA inhibits UCN-01-mediated IL-1β release from FMF patient's monocytes. Monocytes from three FMF patients were primed first with LPS (10ng/ml) during 2.5h and, when indicated, pre-treated with CA (40 nM) during 30 min. Cells were then treated with 12.5 μM UCN-01 for 90min. Mature IL-1β in supernatants as quantified by ELISA is shown. Each symbol presents an average (error bars represent median interquartile range) of three biological replicates for one patient. Kruskal-Wallis test with Dunn's correction for multiple comparisons was applied. P-value less than 0.05 was considered significant; <0.05 (*).

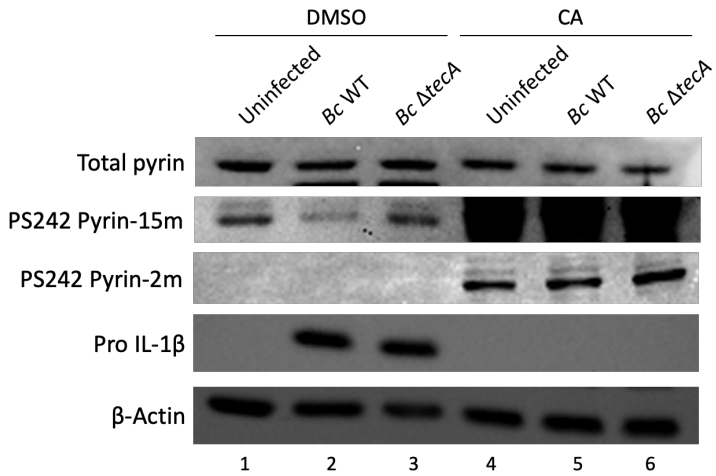

Fig.S3. PPP inhibition with CA results in hyperphosphorylation of pyrin S242. Naïve THP-1 cells were pre-treated for 15 min and maintained with either DMSO or 10nM CA, and either left uninfected or infected with *B. cenocepacia* (Bc) WT or Δ*tecA* for 180 min at an MOI of 20. Immunoblot analysis of total and PS242 pyrin and pro-IL-1β in THP-1 lysates is shown. PS242 pyrin signals are show with long (15m) or short (2m) exposures for comparison. Actin was immunoblotted as a loading control.

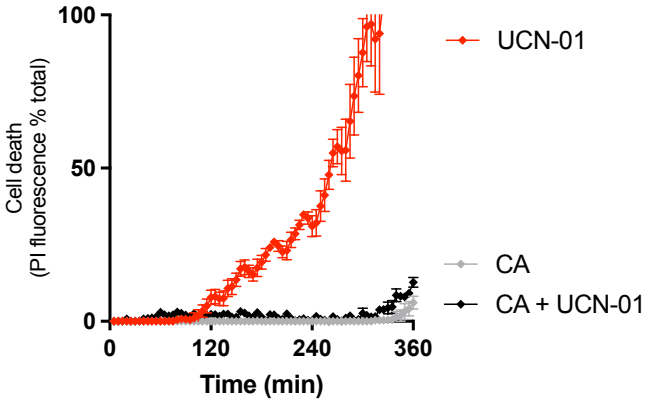

814
815 Fig.S4. CA inhibits UCN-01-mediated cell death in human monocytes expressing M694V pyrin
816 variant. U937 *MEFV*^{KO} cells expressing p.M694V *MEFV* variant were treated with UCN-01 (12.5
817 μM) with or without pre-treatment with Calyculin A (40 nM). Propidium iodide (PI)
818 influx/fluorescence was monitored every 5 min for 6h. Each data group is presented as an average
819 (error bars are standard deviation) of three technical replicates.
820
821
822

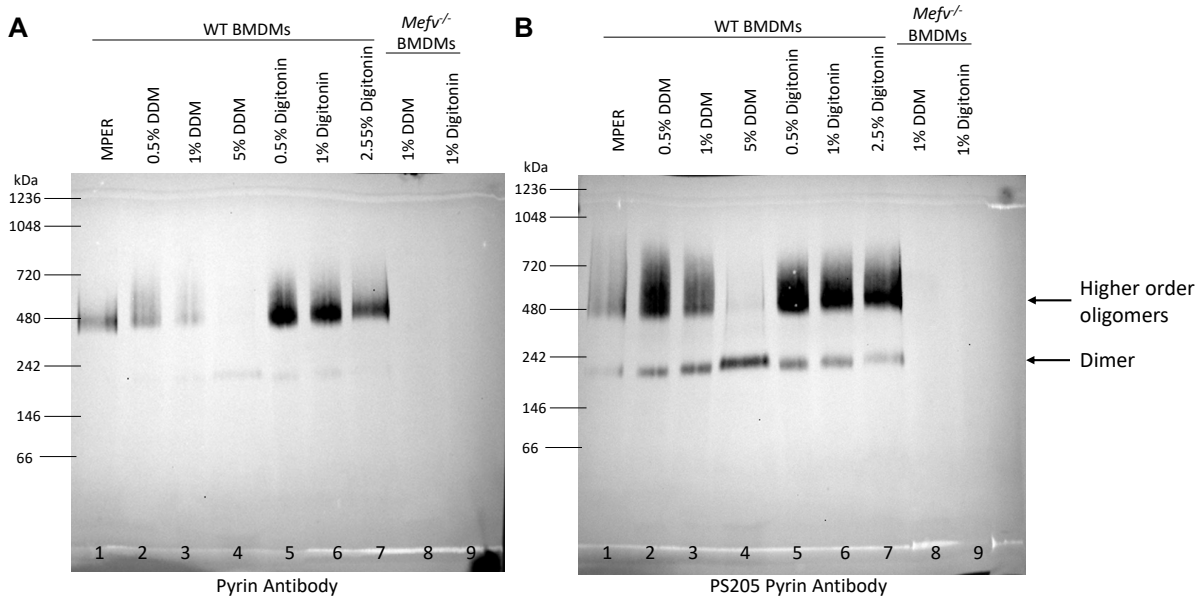

Fig.S5. BMDM lysates prepared with digitonin are optimal for detection of pyrin oligomers using BN-PAGE and immunoblotting. LPS-primed WT and *Mefv*$^{-/-}$ BMDMs were lysed in various non-ionic detergent concentrations as indicated. Lysate samples were separated by BN-PAGE and immunoblotted to visualize total (A) and PS205 pyrin (B) oligomers. Positions of BN-PAGE molecular weight standards are shown on the left of each panel, and dimer and higher order oligomer are indicated on the right of (B).

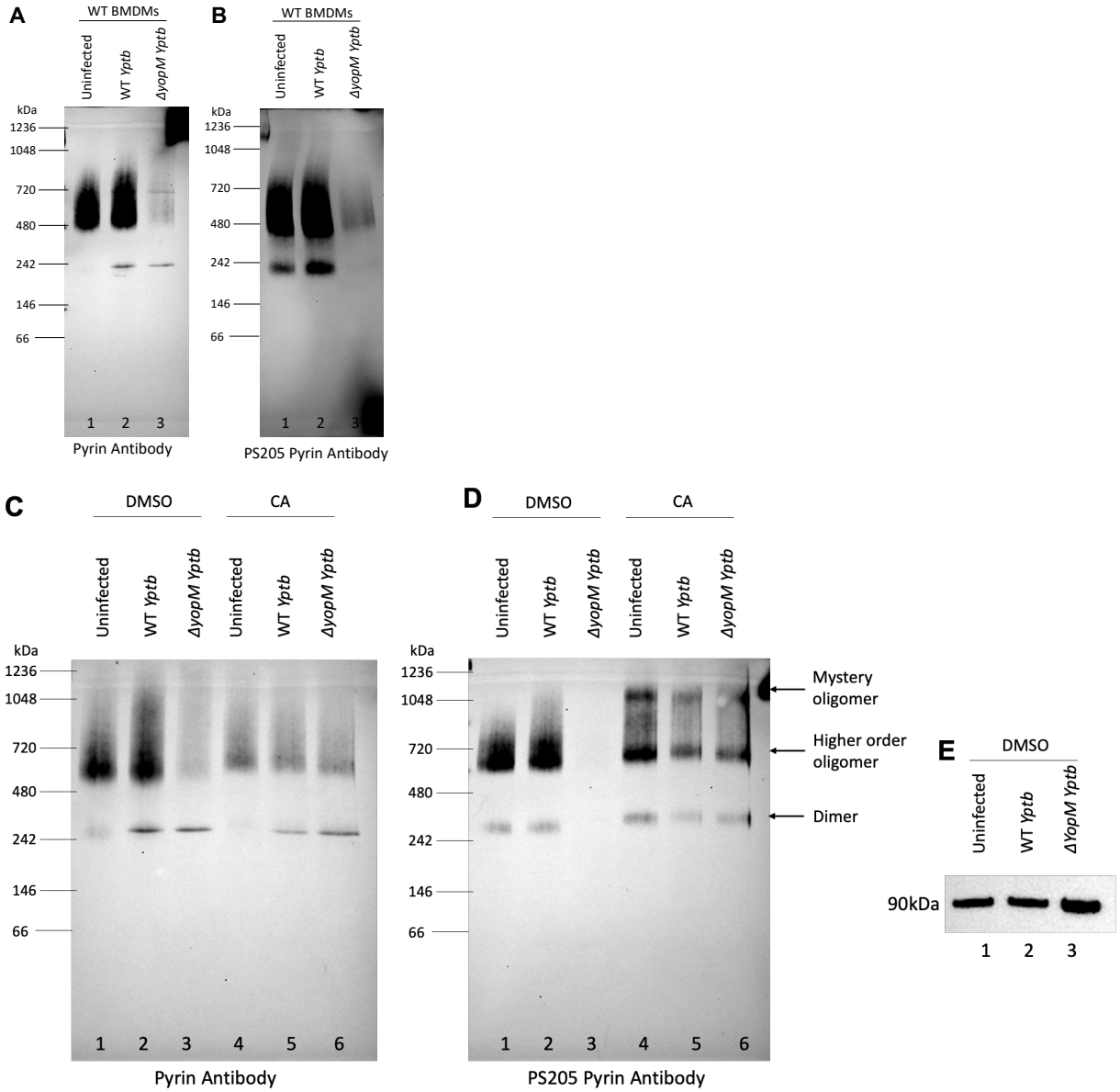

Fig.3. Impact of PPP inhibition with CA and *Yptb* infection on pyrin oligomers and phosphorylation as determined by BN-PAGE and immunoblotting. WT BMDMs left untreated (A,B) or pre-treated and maintained with DMSO or 10 nM CA (C-E) were left uninfected or infected with WT or Δ*yopM Yptb* at an MOI of 30 for 90 mins. BMDM lysate samples prepared in 1% digitonin were separated by BN-PAGE and immunoblotted for total (A,C) or PS205 (B,D) pyrin. BN-PAGE MW standards are shown on the left and tentative positions of pyrin oligomers are shown on the right. Insoluble proteins from 1% digitonin lysates of DMSO treated samples were analyzed by SDS-PAGE and total pyrin immunoblotting (E).

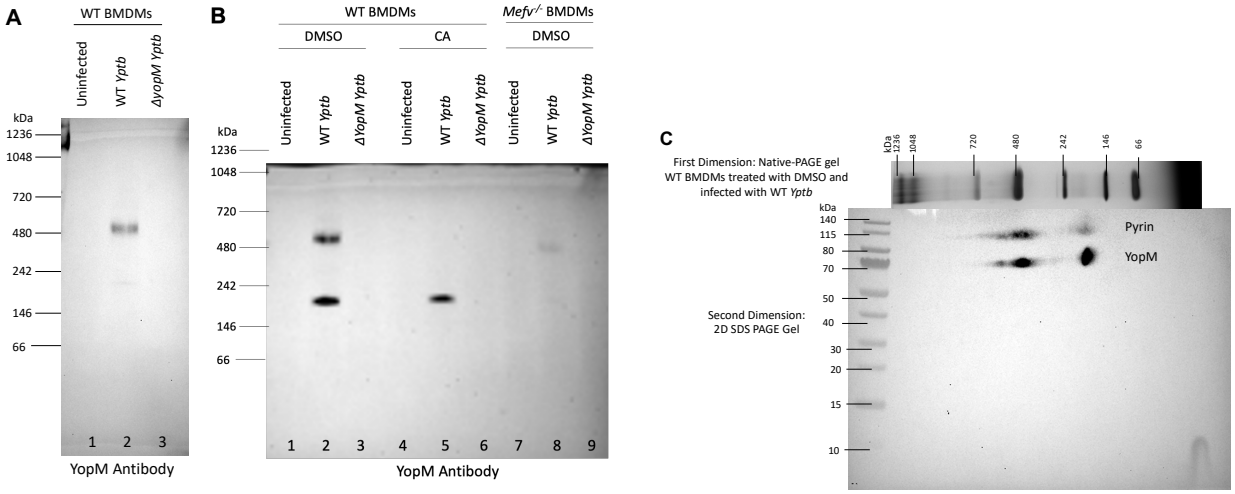

Fig.4. Detection of YopM interaction with pyrin oligomers by one-dimensional and two-dimensional BN-PAGE and immunoblotting. Untreated WT BMDMs (A) or WT or *Mefv*$^{-/-}$ BMDMs pre-treated for 15 min and maintained in DMSO or CA (B, C) were either left uninfected or infected with WT or Δ*yopM Yptb* at an MOI of 30 for 90 mins. Cell lysates were solubilized in 1% digitonin, separated by one dimensional BN-PAGE and immunoblotted for YopM (A,B). BN-PAGE MW standards are shown on the left and tentative positions of YopM oligomers are shown on the right. C) A 1% digitonin sample from WT BMDMS treated with DMSO and infected with WT *Yptb* was separated in the first dimension by BN-PAGE after which the gel slice was isolated and analyzed by SDS-PAGE in the second dimension followed by immunoblotting for pyrin and YopM. MW markers for each dimension are indicated.

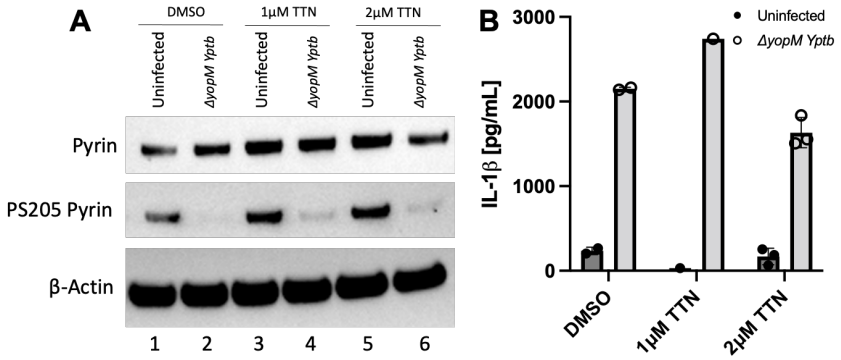

Fig.S6. TTN treatment does not reduce dephosphorylation of pyrin or IL-1β release in BMDMs infected with Δ*yopM Yptb.* LPS-primed BMDMs were pre-treated for 15 mins and maintained with either DMSO or 1 or 2μM TTN and infected with Δ*yopM Yptb* at an MOI of 30 for 90 mins. Treated uninfected BMDMs were analyzed in parallel. A) Immunoblot analysis of PS205 and total pyrin in BMDM lysates. Actin was used as a loading control. B) Mature IL-1β in supernatants as quantified by ELISA. Each data group is presented as an average (error bars are standard deviation) of technical replicates from one experiment.

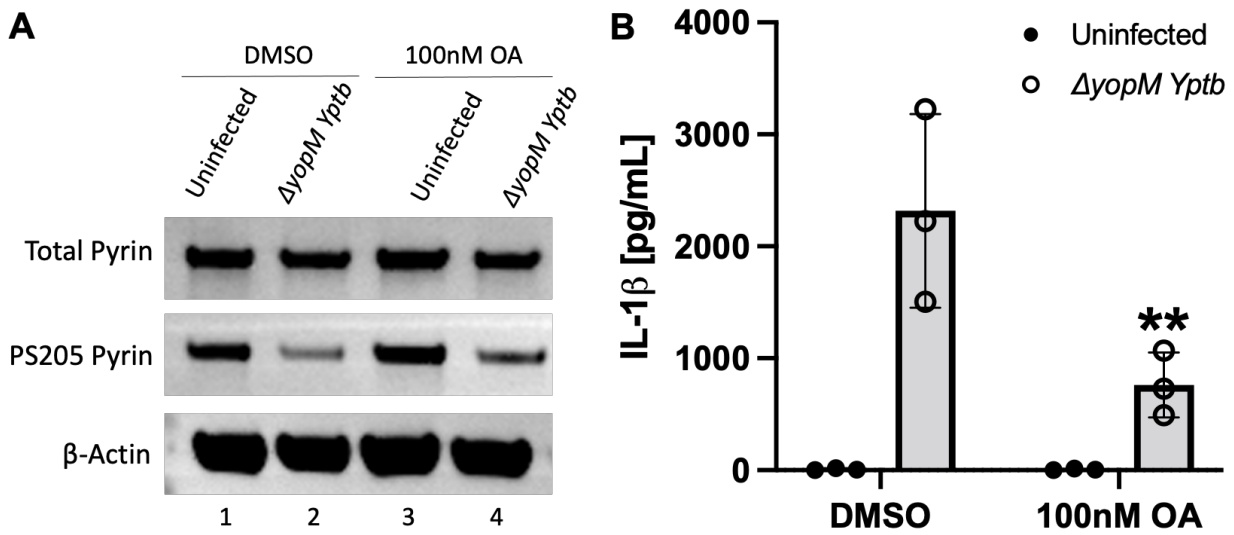

Fig.5. Longer pretreatment with 100nM OA reduces pyrin dephosphorylation and IL-1β release in BMDMs infected with Δ*yopM Yptb.* LPS-primed BMDMs were pre-treated for 3 hrs and maintained with either DMSO or 100nM OA and infected with the Δ*yopM Yptb* at an MOI of 30 for 90 mins. Treated uninfected BMDMs were analyzed in parallel. A) Immunoblot analysis of PS205 and total pyrin in BMDM lysates. Actin was used as a loading control. B) Mature IL-1β in supernatants as quantified by ELISA. Two-way ANOVA with Bonferroni post hoc correction was applied to calculate significance and p-value of OA treatment as compared to its corresponding DMSO treated and Δ*yopM* infected sample is indicated. P-value<0.05 was considered significant; <0.01 (**). Each data group is presented as an average (error bars are standard deviation) of at least 3 independent experiments.

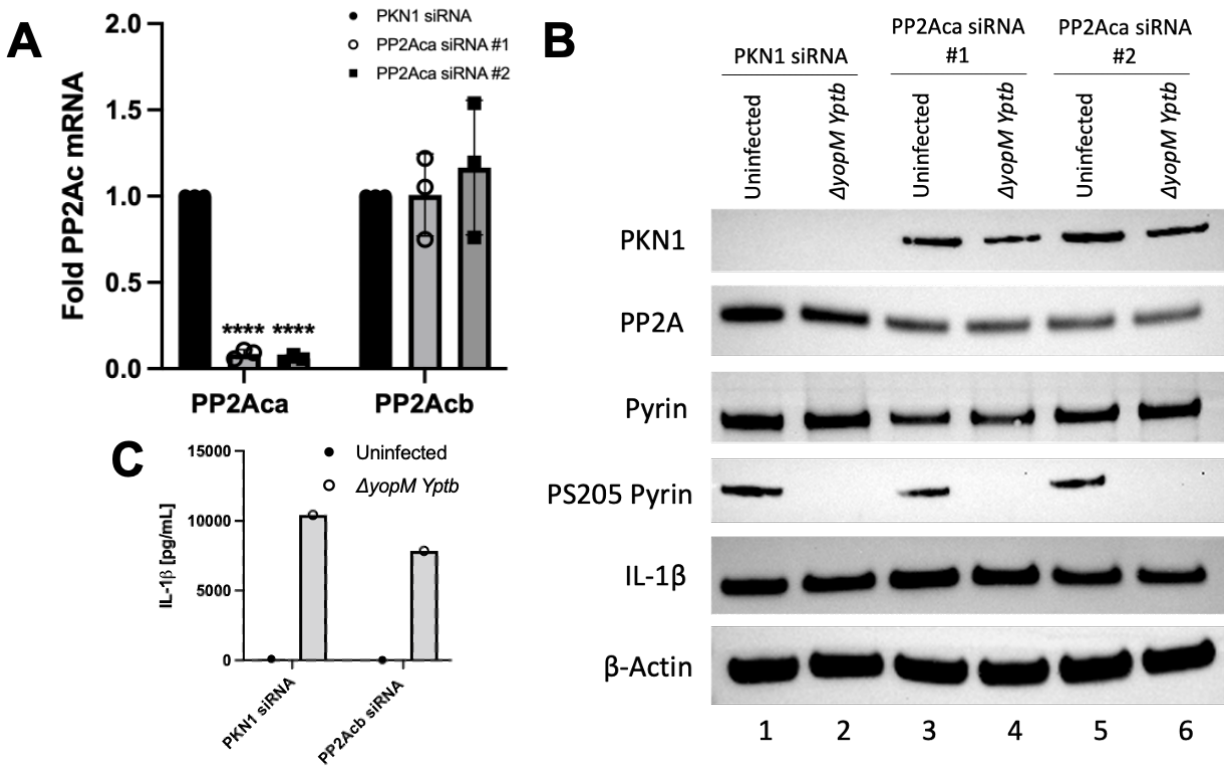

Fig.S6. Individual siRNA knock-down of PP2Aca and PP2Acb in BMDMs does not prevent pyrin inflammasome activation. WT BMDMs were electroporated with siRNAs targeting PKN1 (400pmol), PP2Aca (1000pmol), or PP2Acb (500pmol). 24hr after electroporation the BMDMs were LPS-primed. 48hr following electroporation, cells were either left uninfected or infected with Δ*yopM Yptb* at an MOI of 30 for 90 mins. A) RT-qPCR analysis of mRNA transcripts of PP2Aca and PP2Acb in uninfected BMDMs. Results were normalized to Hprt mRNA levels. Each data group is presented as an average (error bars are standard deviation) of three independent experiments. One-way ANOVA was applied to calculate significance and p-values as compared to PKN1 control siRNA are indicated. P-value<0.05 was considered significant; <0.0001 (****). B) Immunoblot analysis of PKN1, PP2A, total and PS205 pyrin, and pro-IL-1β in uninfected and Δ*yopM Yptb*-infected BMDM lysates. Actin was used as a loading control. C) Mature IL-1β in supernatants as quantified by ELISA from one experiment.

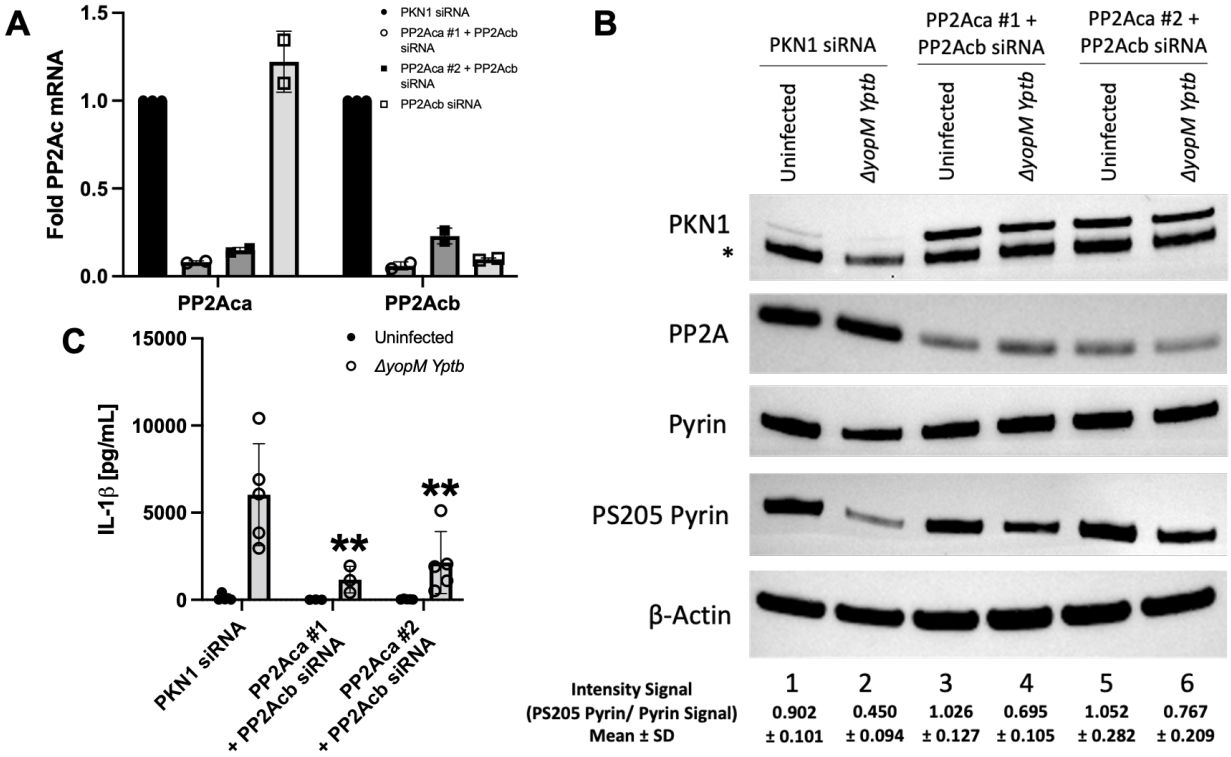

Fig.6. siRNA knock down of PP2A in BMDMs inhibits pyrin S205 dephosphorylation and IL-1β release. WT BMDMs were electroporated with siRNAs targeting PKN1 (400pmol) or PP2Aca + PP2Acb (500pmol each), or PP2Acb (500pmol). 24hr after electroporation the BMDMs were LPS-primed. 48hr following electroporation, cells were either left uninfected or infected with Δ*yopM Yptb* at an MOI of 30 for 90 mins. A) RT-qPCR analysis of mRNA transcripts of PP2Aca and PP2Acb in uninfected BMDMs. Results were normalized to Hprt mRNA levels. Samples with error bars represent standard deviation for an average of two independent experiments. B) Immunoblot analysis of PKN1, PP2A, total and PS205 pyrin in uninfected and Δ*yopM Yptb*-infected BMDM lysates. Actin was used as a loading control. Asterisk (*) indicates bands for total pyrin on an immunoblot that was reprobed for PKN1. Quantified immunoblot band signals representing PS205 pyrin /total pyrin are indicated below lane numbers. Signal of bands from immunoblots from three independent experiments was averaged to calculate mean and standard deviation. C) Mature IL-1β in supernatants as quantified by ELISA. Two-way ANOVA with Bonferroni post hoc correction was applied to calculate significance and p-value of samples as compared to the PKN1 siRNA and Δ*yopM* infected sample is indicated. P-value<0.05 was considered significant; <0.01 (**). Each data group is presented as an average (error bars are standard deviation) of at least 3 independent experiments.

921 REFERENCES
922

923 1. P. Troisfontaines, G. R. Cornelis, Type III secretion: more systems than you think.
924 *Physiology (Bethesda)* **20**, 326-339 (2005).
925 2. B. Raymond *et al.*, Subversion of trafficking, apoptosis, and innate immunity by type III
926 secretion system effectors. *Trends Microbiol* **21**, 430-441 (2013).
927 3. J. M. Blander, L. E. Sander, Beyond pattern recognition: five immune checkpoints for
928 scaling the microbial threat. *Nat Rev Immunol* **12**, 215-225 (2012).
929 4. R. E. Vance, R. R. Isberg, D. A. Portnoy, Patterns of pathogenesis: discrimination of
930 pathogenic and nonpathogenic microbes by the innate immune system. *Cell Host*
931 *Microbe* **6**, 10-21 (2009).
932 5. G. Sollberger, G. E. Strittmatter, M. Garstkiewicz, J. Sand, H. D. Beer, Caspase-1: the
933 inflammasome and beyond. *Innate Immun* **20**, 115-125 (2014).
934 6. S. Shin, I. E. Brodsky, The inflammasome: Learning from bacterial evasion strategies.
935 *Semin Immunol* 10.1016/j.smim.2015.03.006 (2015).
936 7. S. B. Kovacs, E. A. Miao, Gasdermins: Effectors of Pyroptosis. *Trends Cell Biol*
937 10.1016/j.tcb.2017.05.005 (2017).
938 8. J. Shi, W. Gao, F. Shao, Pyroptosis: Gasdermin-Mediated Programmed Necrotic Cell
939 Death. *Trends Biochem Sci* **42**, 245-254 (2017).
940 9. J. Shi *et al.*, Cleavage of GSDMD by inflammatory caspases determines pyroptotic cell
941 death. *Nature* **526**, 660-665 (2015).
942 10. T. Bergsbaken, S. L. Fink, A. B. den Hartigh, W. P. Loomis, B. T. Cookson, Coordinated
943 host responses during pyroptosis: caspase-1-dependent lysosome exocytosis and
944 inflammatory cytokine maturation. *J Immunol* **187**, 2748-2754 (2011).
945 11. S. M. Brewer, S. W. Brubaker, D. M. Monack, Host inflammasome defense mechanisms
946 and bacterial pathogen evasion strategies. *Curr Opin Immunol* **60**, 63-70 (2019).
947 12. G. R. Cornelis, The type III secretion injectisome. *Nat Rev Microbiol* **4**, 811-825 (2006).
948 13. G. I. Viboud, J. B. Bliska, Yersinia outer proteins: role in modulation of host cell signaling
949 responses and pathogenesis. *Annu Rev Microbiol* **59**, 69-89 (2005).
950 14. D. S. Black, J. B. Bliska, The RhoGAP activity of the *Yersinia pseudotuberculosis* cytotoxin
951 YopE is required for antiphagocytic function and virulence. *Mol. Microbiol.* **37**, 515-527
952 (2000).
953 15. F. Shao *et al.*, Biochemical characterization of the *Yersinia* YopT protease: cleavage site
954 and recognition elements in Rho GTPases. *Proc. Natl. Acad. Sci. U.S.A.* **100**, 904-909
955 (2003).
956 16. C. N. LaRock, B. T. Cookson, The Yersinia virulence effector YopM binds caspase-1 to
957 arrest inflammasome assembly and processing. *Cell Host Microbe* **12**, 799-805 (2012).
958 17. L. K. Chung *et al.*, The Yersinia Virulence Factor YopM Hijacks Host Kinases to Inhibit
959 Type III Effector-Triggered Activation of the Pyrin Inflammasome. *Cell Host Microbe* **20**,
960 296-306 (2016).
961 18. D. Ratner *et al.*, The Yersinia pestis Effector YopM Inhibits Pyrin Inflammasome
962 Activation. *PLoS Pathog* **12**, e1006035 (2016).

963 19. I. E. Brodsky *et al.*, A Yersinia Effector Protein Promotes Virulence by Preventing
964 Inflammasome Recognition of the Type III Secretion System. *Cell Host Microbe* **7**, 376-
965 387 (2010).
966 20. E. E. Zwack *et al.*, Inflammasome activation in response to the Yersinia type III secretion
967 system requires hyperinjection of translocon proteins YopB and YopD. *MBio* **6**, e02095-
968 02014 (2015).
969 21. H. S. Malik, J. B. Bliska, The pyrin inflammasome and the Yersinia effector interaction.
970 *Immunol Rev* **297**, 96-107 (2020).
971 22. N. P. Medici, M. Rashid, J. B. Bliska, Characterization of pyrin dephosphorylation and
972 inflammasome activation in macrophages as triggered by the Yersinia effectors YopE
973 and YopT. *Infect Immun* 10.1128/IAI.00822-18 (2019).
974 23. H. Xu *et al.*, Innate immune sensing of bacterial modifications of Rho GTPases by the
975 Pyrin inflammasome. *Nature* **513**, 237-241 (2014).
976 24. D. F. Aubert *et al.*, A Burkholderia Type VI Effector Deamidates Rho GTPases to Activate
977 the Pyrin Inflammasome and Trigger Inflammation. *Cell Host Microbe* **19**, 664-674
978 (2016).
979 25. O. Schnappauf, J. J. Chae, D. L. Kastner, I. Aksentijevich, The Pyrin Inflammasome in
980 Health and Disease. *Front Immunol* **10**, 1745 (2019).
981 26. B. K. Ganser-Pornillos, O. Pornillos, Restriction of HIV-1 and other retroviruses by TRIM5.
982 *Nat Rev Microbiol* **17**, 546-556 (2019).
983 27. C. Weinert, D. Morger, A. Djekic, M. G. Grutter, P. R. Mittl, Crystal structure of TRIM20
984 C-terminal coiled-coil/B30.2 fragment: implications for the recognition of higher order
985 oligomers. *Sci Rep* **5**, 10819 (2015).
986 28. J. W. Yu *et al.*, Pyrin activates the ASC pyroptosome in response to engagement by
987 autoinflammatory PSTPIP1 mutants. *Mol Cell* **28**, 214-227 (2007).
988 29. J. J. Chae *et al.*, Isolation, genomic organization, and expression analysis of the mouse
989 and rat homologs of MEFV, the gene for familial mediterranean fever. *Mamm Genome*
990 **11**, 428-435 (2000).
991 30. W. Gao, J. Yang, W. Liu, Y. Wang, F. Shao, Site-specific phosphorylation and microtubule
992 dynamics control Pyrin inflammasome activation. *Proc Natl Acad Sci U S A* **113**, E4857-
993 4866 (2016).
994 31. J. D. Jones, J. L. Dangl, The plant immune system. *nature* **444**, 323-329 (2006).
995 32. D. Thumkeo, S. Watanabe, S. Narumiya, Physiological roles of Rho and Rho effectors in
996 mammals. *Eur J Cell Biol* **92**, 303-315 (2013).
997 33. Y. H. Park, G. Wood, D. L. Kastner, J. J. Chae, Pyrin inflammasome activation and RhoA
998 signaling in the autoinflammatory diseases FMF and HIDS. *Nat Immunol* **17**, 914-921
999 (2016).
1000 34. Y. H. Park *et al.*, Ancient familial Mediterranean fever mutations in human pyrin and
1001 resistance to Yersinia pestis. *Nat Immunol* 10.1038/s41590-020-0705-6 (2020).
1002 35. S. L. Masters *et al.*, Familial autoinflammation with neutrophilic dermatosis reveals a
1003 regulatory mechanism of pyrin activation. *Sci Transl Med* **8**, 332ra345 (2016).
1004 36. M. W. McCoy, M. L. Marre, C. F. Lesser, J. Mecsas, The C-terminal tail of Yersinia
1005 pseudotuberculosis YopM is critical for interacting with RSK1 and for virulence. *Infect*
1006 *Immun* **78**, 2584-2598 (2010).

1007 37. Y. Jamilloux, F. Magnotti, A. Belot, T. Henry, The pyrin inflammasome: from sensing
1008 RhoA GTPases-inhibiting toxins to triggering autoinflammatory syndromes. *Pathogens*
1009 *and disease* **76**, fty020 (2018).
1010 38. F. Magnotti *et al.*, Pyrin dephosphorylation is sufficient to trigger inflammasome
1011 activation in familial Mediterranean fever patients. *EMBO Mol Med* **11**, e10547 (2019).
1012 39. I. Nasa, A. N. Kettenbach, Coordination of Protein Kinase and Phosphoprotein
1013 Phosphatase Activities in Mitosis. *Front Cell Dev Biol* **6**, 30 (2018).
1014 40. K. Aktories, Bacterial protein toxins that modify host regulatory GTPases. *Nat Rev*
1015 *Microbiol* **9**, 487-498 (2011).
1016 41. A. N. Namboodiripad, M. L. Jennings, Permeability characteristics of erythrocyte
1017 membrane to okadaic acid and calyculin A. *American Journal of Physiology-Cell*
1018 *Physiology* **270**, C449-C456 (1996).
1019 42. A. Stutz *et al.*, NLRP3 inflammasome assembly is regulated by phosphorylation of the
1020 pyrin domain. *J Exp Med* **214**, 1725-1736 (2017).
1021 43. M. A. Gavrilin *et al.*, Activation of the pyrin inflammasome by intracellular Burkholderia
1022 cenocepacia. *J Immunol* **188**, 3469-3477 (2012).
1023 44. Y. Jamilloux *et al.*, Familial Mediterranean fever mutations are hypermorphic mutations
1024 that specifically decrease the activation threshold of the Pyrin inflammasome.
1025 *Rheumatology (Oxford)* **57**, 100-111 (2018).
1026 45. I. Wittig, H. P. Braun, H. Schagger, Blue native PAGE. *Nat Protoc* **1**, 418-428 (2006).
1027 46. E. M. Kofoed, R. E. Vance, Blue native polyacrylamide gel electrophoresis to monitor
1028 inflammasome assembly and composition. *Methods Mol Biol* **1040**, 169-183 (2013).
1029 47. M. S. Choy *et al.*, PP1: Tautomycetin complex reveals a path toward the development of
1030 PP1-specific inhibitors. *Journal of the American Chemical Society* **139**, 17703-17706
1031 (2017).
1032 48. S. Mitsuhashi *et al.*, Tautomycetin is a novel and specific inhibitor of serine/threonine
1033 protein phosphatase type 1, PP1. *Biochemical and biophysical research communications*
1034 **287**, 328-331 (2001).
1035 49. P. Kreienbuhl, H. Keller, V. Niggli, Protein phosphatase inhibitors okadaic acid and
1036 calyculin A alter cell shape and F-actin distribution and inhibit stimulus-dependent
1037 increases in cytoskeletal actin of human neutrophils. (1992).
1038 50. M. Swingle, L. Ni, R. E. Honkanen, "Small-molecule inhibitors of Ser/Thr protein
1039 phosphatases" in Protein Phosphatase Protocols. (Springer, 2007), pp. 23-38.
1040 51. Y. Shi, Serine/threonine phosphatases: mechanism through structure. *Cell* **139**, 468-484
1041 (2009).
1042 52. N. M. Luheshi, J. A. Giles, G. Lopez-Castejon, D. Brough, Sphingosine regulates the
1043 NLRP3-inflammasome and IL-1β release from macrophages. *European journal of*
1044 *immunology* **42**, 716-725 (2012).
1045 53. I. Jeru *et al.*, Interaction of pyrin with 14.3.3 in an isoform-specific and phosphorylation-
1046 dependent manner regulates its translocation to the nucleus. *Arthritis Rheum* **52**, 1848-
1047 1857 (2005).
1048 54. A. G. Evdokimov, D. E. Anderson, K. M. Routzahn, D. S. Waugh, Unusual molecular
1049 architecture of the Yersinia pestis cytotoxin YopM: a leucine-rich repeat protein with the
1050 shortest repeating unit. *J Mol Biol* **312**, 807-821 (2001).

1051 55. C. MacKintosh, K. A. Beattie, S. Klumpp, P. Cohen, G. A. Codd, Cyanobacterial
1052 microcystin-LR is a potent and specific inhibitor of protein phosphatases 1 and 2A from
1053 both mammals and higher plants. *FEBS letters* **264**, 187-192 (1990).
1054 56. L. Mao *et al.*, Bruton tyrosine kinase deficiency augments NLRP3 inflammasome
1055 activation and causes IL-1β–mediated colitis. *The Journal of clinical investigation* **130**,
1056 1793-1807 (2020).
1057 57. M. Simonet, S. Falkow, Invasin expression in *Yersinia pseudotuberculosis*. *Infect. Immun.*
1058 **60**, 4414-4417 (1992).
1059 58. J. B. McPhee, P. Mena, J. B. Bliska, Delineation of regions of the Yersinia YopM protein
1060 required for interaction with the RSK1 and PRK2 host kinases and their requirement for
1061 interleukin-10 production and virulence. *Infect Immun* **78**, 3529-3539 (2010).
1062 59. L. K. Chung *et al.*, IQGAP1 is important for activation of caspase-1 in macrophages and is
1063 targeted by Yersinia pestis type III effector YopM. *MBio* **5**, e01402-01414 (2014).
1064 60. N. A. Loeven *et al.*, The Burkholderia cenocepacia Type VI Secretion System Effector
1065 TecA Is a Virulence Factor in Mouse Models of Lung Infection. *mBio* **12**, e0209821
1066 (2021).
1067 61. J. J. Chae *et al.*, Targeted disruption of pyrin, the FMF protein, causes heightened
1068 sensitivity to endotoxin and a defect in macrophage apoptosis. *Mol Cell* **11**, 591-604
1069 (2003).
1070 62. B. Lagrange *et al.*, Human caspase-4 detects tetra-acylated LPS and cytosolic Francisella
1071 and functions differently from murine caspase-11. *Nature communications* **9**, 1-14
1072 (2018).
1073 63. K. L. Meerbrey *et al.*, The pINDUCER lentiviral toolkit for inducible RNA interference in
1074 vitro and in vivo. *Proceedings of the National Academy of Sciences* **108**, 3665-3670
1075 (2011).
1076 64. C. L. Case, C. R. Roy, Asc modulates the function of NLRC4 in response to infection of
1077 macrophages by Legionella pneumophila. *MBio* **2**, e00117-00111 (2011).
1078 65. R. Pierini *et al.*, AIM2/ASC triggers caspase-8-dependent apoptosis in Francisella-
1079 infected caspase-1-deficient macrophages. *Cell Death & Differentiation* **19**, 1709-1721
1080 (2012).
1081